MANCHESTER 1824
The University of Manchester

Uncertainty of CFD Predictions of Boiling in a Nuclear Reactor Fuel Channel

A dissertation submitted to The University of Manchester for the degree of

Master of Science in Thermal Power and Fluid Engineering

in the Faculty of Science and Engineering

Year of submission

2023

Student ID

11106116

The School of Engineering

Contents

Word count: 12095

List of figures

List of tables

Abstract

Anticipating the boiling behavior within nuclear reactor fuel channels stands as a pivotal challenge in the design of nuclear reactors. Modern reactors rigorously adhere to strict standards and manufacturing protocols to prevent safety hazards. These measures are a direct outcome of exhaustive experiments, analyses, and decision-making frameworks that deliberate over the complex flow phenomena and heat transfer transpiring under highly transient conditions within the nuclear reactor.

A pivotal tool employed for analysing these phenomena is Computational Fluid Dynamics (CFD), particularly within the realm of multi-phase simulations. This tool offers a robust approach to investigate and model these phenomena, albeit within a controlled level of approximation. Consequently, these simulations inherently perform with assorted sources of uncertainty due to the nature of the relevant physical processes and the inherent limitations of numerical techniques.

Consequently, an imperative need to meticulously study and simulate reactor conditions is observed to ensure operational safety. This includes assessing the statistical uncertainty associated with parameters and simulation outcomes relevant to these conditions. This work hopes to study the prevalent CFD simulations within the scope of wall boiling in nuclear reactors. Moreover, it seeks to elaborate upon the uncertainty introduced into operating parameters, which is subsequently carried forward through uncertainty quantification methodologies. These methodologies are implemented compute the upper limits of peak cladding temperatures during reactor operations. This is crucial in determining the accuracy of the CFD estimates and to prevent single estimates of unknown accuracy, given by a subjective choice of CFD models.

Declaration

I hereby confirm that this dissertation is my own original work unless referenced clearly to the contrary, and that no portion of the work referred to in the dissertation has been submitted in support of an application for another degree or qualification of this or any other university or other institute of learning.

Intellectual property statement

i The author of this thesis (including any appendices and/or schedules to this thesis) owns certain copyright or related rights in it (the "Copyright") and s/he has given The University of Manchester certain rights to use such Copyright, including for administrative purposes.

ii Copies of this thesis, either in full or in extracts and whether in hard or electronic copy, may be made *only* in accordance with the Copyright, Designs and Patents Act 1988 (as amended) and regulations issued under it or, where appropriate, in accordance with licensing agreements which the University has from time to time. This page must form part of any such copies made.

iii The ownership of certain Copyright, patents, designs, trademarks and other intellectual property (the "Intellectual Property") and any reproductions of copyright works in the thesis, for example graphs and tables ("Reproductions"), which may be described in this thesis, may not be owned by the author and may be owned by third parties. Such Intellectual Property and Reproductions cannot and must not be made available for use without the prior written permission of the owner(s) of the relevant Intellectual Property and/or Reproductions.

iv Further information on the conditions under which disclosure, publication and commercialisation of this thesis, the Copyright and any Intellectual Property and/or Reproductions described in it may take place is available in the University IP Policy (see `http://documents.manchester.ac.uk/DocuInfo.aspx?DocID=24420`), in any relevant Dissertation restriction declarations deposited in the University Library, and The University Library's regulations (see `http://www.library.manchester.ac.uk/about/regulations/_files/Library-regulations.pdf`).

Acknowledgements

I extend my profound gratitude to my esteemed supervisor, Dr. Giovanni Giustini, whose unwavering guidance and support have been critical in the successful completion of this research endeavor. His expertise and constant encouragement provided the foundation for my growth and development. I would like to convey my sincere gratitude and admiration for the invaluable guidance and support he provided at the final stage of this project. His own work and understanding towards boiling phenomena has been crucial and tantamount to a comprehensive investigation in this work. This journey would have been significantly more challenging without his invaluable suggestions and constructive feedback, which propelled my work to new heights.

I also want to express my appreciation to my peers at the University of Manchester. Their camaraderie, insightful discussions, and shared academic enthusiasm have been enriching. Together, we've tackled challenges, exchanged ideas, and fostered a collaborative environment that significantly influenced the quality of this research.

Lastly, heartfelt thanks go to my family, who have been a pillar of support throughout every step of this academic pursuit. Their unwavering belief in me has been a driving force, and I am truly grateful for their constant encouragement.

1 Introduction

In nuclear reactor setups, boiling flow regimes are often useful as, in bubbly flows heat transfer rates are often high even for minimal temperature differences.[1] However, bubbly flows add complexity to estimation of critical parameters through simulation techniques like CFD. In a nuclear reactor fuel channel, fluid flow is subcooled and is characterized by high heat transfer and wall boiling flow regimes.[2][3] Due to heat transfer from the fuel channel walls, we observe that boiling progresses as a characteristic of location on the subchannel subject to system design. Three classifications of boiling flow can be made in both annular flow and flows in vertical tubes; subcooled flows, subcooled nucleate boiling and saturated bubbly flows after departure from nucleate boiling (DNB) as shown in figure 1.[4]

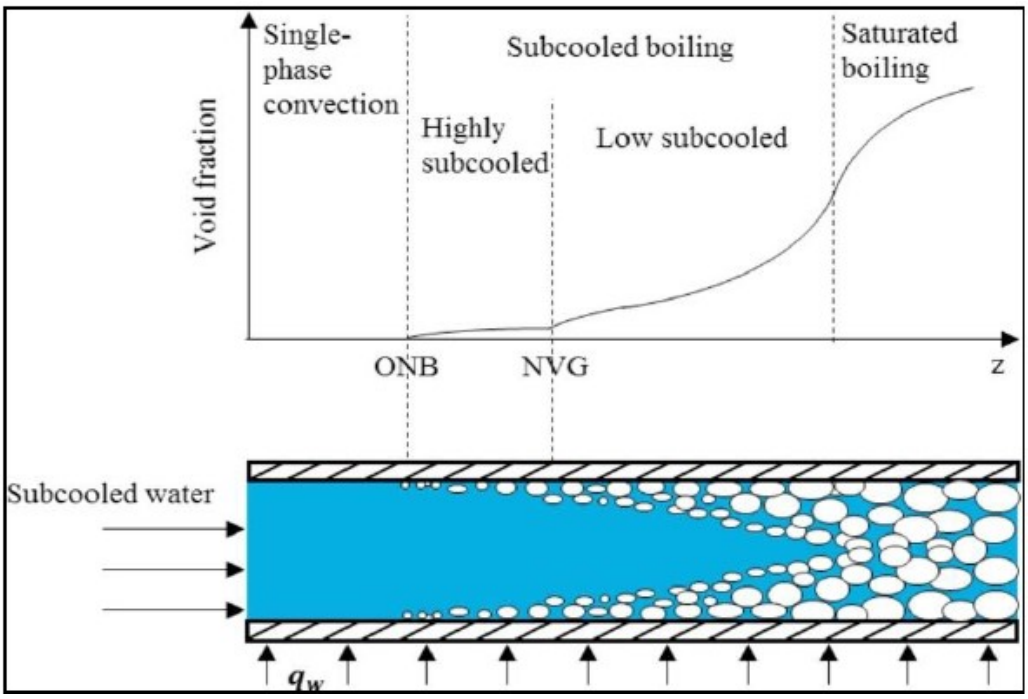

Fig. 1. Stages of boiling in a reactor fuel channel depicted with onset of nucleate boiling and net vapour generation stages.[4]

It is crucial to establish the geometrical scope, which in the case of this work, is at component scale, as well as to implement accurate models on CMFD that successfully estimate all flow conditions in the regime [5].

Moreover, the results from these models should be valid against pre-existing experimental data, for the particular regime. The imperfect accuracy of these models give rise to the scope for uncertainty analysis as CFD calculations cannot perfectly emulate reactor transient conditions due to the subjective capabilities of the model and absence of mature mechanistic models at the microscale level. [6] Hence, uncertainty quantification should be done on applications where single CFD estimates with unknown accuracy (and precision for clustered CFD data) is not satisfactory. This quantification is done with the help of statistical tools and the GRS model used in the industry.

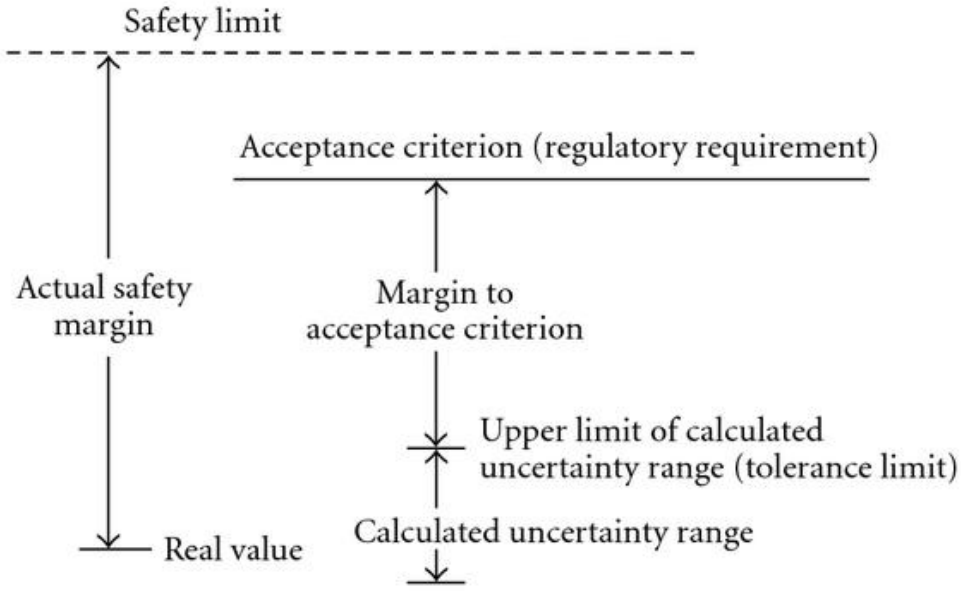

Fig. 2. Margins of peak cladding temperatures of a nuclear reactor fuel channel as observed for UQ by GRS method.[7]

1.1 Background And Motivation

Nuclear reactors are a modern engineering marvel that play a crucial role in meeting the global demand for clean and sustainable power generation. Computational Fluid Dynamics (CFD) has emerged as an important tool for analyzing complex fluid flow and heat transfer phenomena within nuclear reactor fuel channels. Understanding this relation between fluid dynamics, heat transfer, and nuclear processes is critical for en-

suring the safety and performance of nuclear reactors. In particular, boiling phenomena within fuel channels significantly influence reactor operation, construction and safety standards. As nuclear reactors are developed and the operating conditions are harsher, accurate predictions of boiling in fuel channels are essential for implement safety margins, improving reactor efficiency, and reducing operational costs.

From the numerous concerns above, avoiding a nuclear reactor accident is the primary concern of any decision-making systems. For those purposes, standards and regulations are put in place for reactor safety for its design and subsequent operations inclusive of any reactor design. [8]

Despite the potential benefits of utilizing CFD for predicting boiling phenomena in nuclear reactor fuel channels, several challenges and uncertainties remain. The inherent complexity of multiphase flow and heat transfer, coupled with the diverse range of physical processes occurring simultaneously, poses significant computational and modeling challenges. Additionally, factors such as wall surface conditions, turbulence, phase change dynamics, and interfacial interactions introduce uncertainties that can propagate through the simulation, impacting the accuracy of predictions.[9][10]

The accurate prediction of boiling phenomena in nuclear reactor fuel channels requires propagating the uncertainties present in CFD simulations. Uncertainties can arise from various sources, including modeling assumptions, parameter variations, and numerical approximations. Incorporating Uncertainty Quantification (UQ) techniques into CFD simulations provides a systematic framework for characterizing and managing uncertainties. UQ enables the estimation of the impact of various sources of uncertainty on the final simulation results and their sensitivity towards the final peak cladding temperatures, enabling predictions with a higher statistical confidence.[11]

It can be noted that for the purposes of this work, Computational Multi phase Fluid

Dynamics (CMFD) and Computational Fluid Dynamics (CFD) are largely interchangeable, but CMFD has been used where the methodology is directly applicable to multiphase modelling and simulation.

1.2 Objectives

The aims of this study are twofold, centered on the development of a Computational Fluid Dynamics (CFD) model and the execution of uncertainty quantification for predicting wall boiling phenomena within nuclear reactor fuel channels. The primary aim of this study revolves around the construction of a CFD simulation that reproduces the heat transfer dynamics present in reactor fuel channels. Subsequently, a UQ model is established, focusing on boiling heat transfer and aiming to predict boiling conditions through statistical methods.

The initial phase of this research centers on modelling the CFD simulation with a focus on capturing the complexities of two-phase heat transfer within a reactor subchannel, putting into focus a macroscopic model. By achieving this, the simulation strives to provide a dependable depiction of the heat transfer mechanisms and the fluid flow regime on a component level scale.

Next is the systematic process of uncertainty quantification. This entails a systematic analysis of the uncertainties and variations embedded within the model's input parameters and underlying assumptions. By subjecting the model to a spectrum of potential uncertainties, the study achieves a comprehensive understanding of the fluid mechanics in operation. This, in turn, leads to the estimation of the maximum wall cladding temperatures under varying conditions. This estimation offers then propogates into the model's sensitivity using the GRS UQ method, particularly in the context of wall boiling.

In conclusion, this study hopes to achieve the following objectives:

- Review the state-of-the-art CFD modeling approaches for simulating boiling in nuclear reactor fuel channels.
- Identify sources of uncertainties in CFD simulations of boiling phenomena and analyse their impact on simulation results.
- Develop and implement uncertainty quantification techniques relevant to multi-phase flow and heat transfer simulations.
- Apply the developed methodologies to operating conditions and parameters in nuclear reactor fuel channels.
- Analyze the effects of uncertainties on prediction accuracy and safety margins, and to predict upper limits of peak cladding temperatures within the reactor channel

1.3 Report structure

This work is divided into 6 chapters focusing on the various aspects of the conducted investigation.

Chapter 2 focuses on a comprehensive literature review of computational multi phase dynamics modelling that has been used for the purposes of two phase Eulerian modelling and the various approaches that have been taken to tackle boiling as a problem statement in modelling research. It also includes a review of the uncertainty quantification methods deployed for the purposes of estimating final predictions from the results of the CFD model.

Chapter 3 focuses on the methodology and the systematic approach followed for the this work including an indepth view of the mathematics and physics behind the CFD

code,the statistics involved and the final UQ and sensitivity analysis framework.

Chapter 4 discusses the results obtained from performing the above mentioned analysis and the insights given by the tools that have been used for wall boiling in the reactor channel and subsequent UQ.

Chapter 5 summarizes the investigation in this report and looks at final conclusions drawn out from the results and presents them in a thematic manner.

Chapter 6 identifies any research scopes and gaps that have been realized in the due course of this investigation and points them out for the development of problem statements relevant to boiling of coolants in a nuclear reactor channel.

2 Literature review

2.1 Introduction

In the intricate realm of nuclear engineering, the accurate and reliable prediction of heat transfer phenomena within nuclear reactor fuel channels is paramount to the safe and efficient operation of these critical energy-producing systems. Within this context, the phenomenon of wall boiling, characterized by the formation and growth of vapor bubbles at the fuel channel wall due to intense localized heat fluxes, represents a pivotal aspect of nuclear reactor thermal-hydraulic analysis.[1]

2.2 CFD Modelling

Boiling is a complex phenomenon that occurs in nuclear reactor fuel channels due to the high heat fluxes experienced by the fuel rods. It can manifest in various forms, including

nucleate boiling, film boiling, and critical heat flux (CHF). Accurate prediction of these boiling regimes is crucial for maintaining the desired coolant temperatures, preventing fuel overheating, and ensuring the structural integrity of the reactor components.

Eulerian-Eulerian modeling is a widely adopted approach for simulating multiphase flows, especially those involving boiling and condensation in nuclear reactor systems. This modeling approach treats each phase (e.g., liquid and vapor) as separate continuous phases within a computational domain, where interphase interactions and phase change phenomena are explicitly accounted for. The key equations governing mass, momentum, and energy conservation for each phase are solved concurrently, enabling detailed predictions of phase distribution, interfacial phenomena, and heat transfer. Within this model, the liquid and vapor phases are treated as separate but interpenetrating continua, allowing for the representation of a wide range of flow patterns commonly encountered in boiling channels. The model's strength lies in its capacity to account for continuous interfacial dynamics between these phases, enabling the accommodation of slug flows, bubbly flows, and other intricate flow patterns characteristic of boiling phenomena.

Many other strategies exist for modelling wall boiling in nuclear reactors and other applications, and boiling models do exist which are more suitable for non-Eulerian Eulerian methods like Volume of Fluid or CFD codes that are Lagrangian in nature, due to the level of fidelity involved in the simulation and the scope of the simulation being macroscopic or microscopic. [5]

The study by Colombo and Fairweather (2016)[12] presented a comprehensive investigation into the accuracy of Eulerian–Eulerian, models predicting subcooled boiling flows. These models have shown promise in capturing the complex interplay between vapor and liquid phases, as well as the intricate heat transfer mechanisms during boiling. The authors evaluated various modeling approaches, including the interfacial area den-

sity (IAD) approach, and the two-group interfacial area transport equation, highlighting the significance of accurate interfacial area prediction in improving boiling simulations.

Importance lies in regulating high fuel channel temperatures in nuclear engineering to secure safety and integrity of reactors. According to Hózer (2014), maintaining temperatures below a specific acceptance criterion is crucial, driven by the need to avoid the leakage of fission fuel products. A possible consequence of fuel rod overheating is a weakening of structural integrity, which could lead to a radioactive release or containment breach.[13]

The paper by Han et al.[14] discusses the verification and validation of CFD simulations for pressurized water reactor (PWR) fuel assembly analysis. It emphasizes the importance of accurate numerical models, grid resolution, and turbulence modeling in obtaining reliable predictions of thermal-hydraulic parameters. A PWR rod bundle geometry was put forward and CFD simulations were run and validated against existing experimental data for mixing vane spacer grids on an Eulerian Eulerian framework. CFD tests were also run to predict flow regime behaviour with a critical heat flux criterion (CHF) for similar geometry and operating conditions [15], further reinforcing the versatility of the Eulerian modelling method.

As elucidated by Yadigaroglu [16], this imperfection arises primarily from the inability of CFD calculations to precisely emulate reactor transient conditions. Several factors contribute to this limitation.

First and foremost, the subjectivity inherent to CFD models cannot be overstated. These models rely on a set of governing equations, turbulence models, and boundary conditions, each of which involves certain assumptions and simplifications. These assumptions are necessary to make the complex computational problem tractable but inherently introduce an element of uncertainty into the predictions.

Furthermore, the absence of mature mechanistic models at the microscale level compounds the uncertainty in CFD predictions. Wall boiling involves highly dynamic processes at the interface between liquid and vapor phases, where nucleation, bubble growth, coalescence, and departure play pivotal roles. Developing mechanistic models capable of capturing these intricate microscale phenomena is a formidable challenge. In the absence of such models, CFD simulations resort to empirical correlations and closure models, introducing additional sources of uncertainty.[17] Here we put the heat transfer regime applicable to wall boiling as a source of uncertainty into investigation.

The Kurul-Podolski Wall heat flux partitioning (WHFP) boiling heat transfer model [18] is built upon the premise that the heat transfer during boiling can be divided into three key components: forced convective boiling, nucleate boiling, and film boiling. The resultant then defined the heat flux from the wall to the fluid to be split into three parts: convective heat flux, evaporative heat flux and quenching heat flux as shown in figure 3.

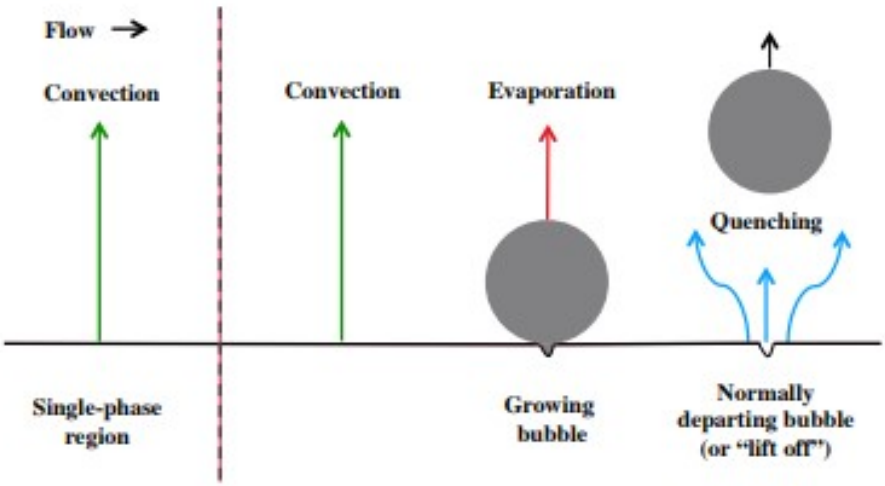

Fig. 3. Partitioning of heat flux into its constituent components and a representation of the physical significance of each of the components [19]

The model combines existing correlations for each component to create a unified prediction tool. Mathematically, the model is represented as follows:

2.2.1 Convective Boiling Heat Flux (q_{conv})

This component of the RPI model is used to estimate heat flux that concerns convective heat transfer from the wall directly to the liquid regime, mathematically simplifying to a single phase heat transfer model. The heat flux for convection is obtained by applying Newton's law of cooling[20] with the boiling fraction area that is not influenced by the vapour (1- A_b). The equation is given as:

$$q_{\text{conv}} = h_{\text{conv}}(1 - \cdot A_b) \cdot (T_{\text{wall}} - T_{\text{bulk}}) \tag{1}$$

where $h_{\text{convection}}$ is the local convective heat transfer coefficient. The equation expresses a linear relationship between the temperature difference between fluid bulk temperature and temperature of wall and the heat flux.

2.2.2 Evaporation (Nucleate Boiling) Heat Flux (q_{evap})

Nucleate boiling is characterized by the formation and growth of vapor bubbles on the heated surface. The heat transfer due to nucleate boiling can be estimated using empirical correlations based on the bubble dynamics and size. A common correlation is the Bowring correlation[21] given as:

$$q_{\text{evap}} = N_a f_b \left(\frac{\pi \cdot d_b^3}{6} \right) \rho_d h_{LV} \tag{2}$$

2.2.3 Quenching Heat Flux (q_{quench})

Quenching heat flux represents the maximum heat flux that can be safely transferred from the wall without triggering dryout, a condition where the wall becomes devoid of liquid coolant. When bubble departure is observed, cooler fluid from the neighbouring region flows into the departure area and fills it enhancing heat transfer. Predicting the QHF accurately is essential for maintaining the integrity of the fuel channel and avoiding potential overheating and fuel failure.The correlation for QHF has been modelled in the correlation[22] by applying Newton's law cooling to the area fraction for vapour as:

$$q_{\text{quench}} = h_{\text{quench}} \cdot A_b \cdot (T_{\text{wall}} - T_{\text{bulk}}) \tag{3}$$

The bubble induced quenching heat transfer coefficient has been given by the correlation by Del Valle and Kenning[23] as:

$$h_{\text{quench}} = 2\lambda_c f_B \sqrt{\frac{\rho_c c_{pc} T_w}{\pi \lambda_c}} \tag{4}$$

2.2.4 Total Heat Flux (q_{total})

The total heat flux at the wall is the sum of these individual heat flux components:

$$q_{\text{total}} = q_{\text{conv}} + q_{\text{evap}} + q_{\text{quench}} \tag{5}$$

RPI WFHP is a very robust heat transfer model [24] that does require to work in conjunction with a few other models that concisely describe the physical wall boiling

process. These models are also implemented in the investigation of the uncertainty in the models and form a crucial part of the methodology, in which modelling of the reactor sub-channel is explored.

2.3 Sensitivity Analysis and Uncertainty Quantification

This section presents the methodology adopted for uncertainty quantification using the GRS (Gläser's approach) method [7] in the context of uncertainty assessment for Computational Fluid Dynamics (CFD) predictions of wall boiling in a nuclear reactor fuel channel. The objective is to comprehensively evaluate and quantify uncertainties inherent in CFD simulations, providing insights into the reliability and accuracy of these predictions for critical applications.

The general methodology followed for uncertainty quantification of the CFD predictions follows steps deployed as part of nuclear safety analysis as shown in figure 4 As

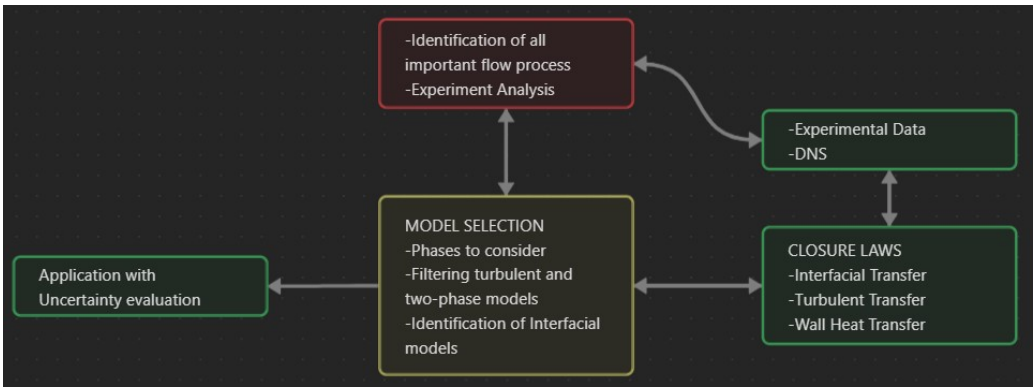

Fig. 4. General Methodology followed for 2 phase multi fluid flow regime used for Nuclear Reactor Safety Analysis (Adapted from [8])

mentioned before, the primary goal of this study is to assess the uncertainties associated with CFD predictions of wall boiling in a nuclear reactor fuel channel. This involves simulating the multiphase flow and heat transfer phenomena occurring within the channel under various operational conditions. The aim is to identify sources of uncertainty and assess their influence on simulation results. The methodology adopted here for UQ

followed here is a method called the Gesellschaft für Anlagen-und Reaktorsicherheit method or the Global Research for Safety method (GRS), proposed by Glaeser in 2008. [7]

GRS has been proposed as a viable option for uncertainty quantification in multiple literature regarding the modelling of nuclear reactor coolant channels along with other methodologies like Monte Carlo and deterministic sampling. In this work, the Monte Carlo method is used where sampling is done from a distribution function to gain a samples of the input parameters that are then propagated through a surrogate, in this case the CFD model. The method makes use of the Wilks law, a non-parametric sampling method, where the number of samples is independent of the parameter or its distribution.[25]

The GRS Wilks non parametric method gives a less conservative estimate compared to government regulations and previous codes, like ATHLET[26] that have been used for UQ of the transient reactor conditions.[7] Moreover, accuracy of the method can be increased with the number of simulations to achieve a higher tolerance with greater confidence simulaneously, which is recommended for reactor systems.[25][27]

To initiate the uncertainty quantification process, a set of uncertain input parameters is identified. These parameters encompass geometrical properties, material properties, initial/boundary conditions, and operational parameters. The uncertainties associated with these inputs arise from manufacturing tolerances, measurement errors, and inherent variability in operating conditions.

Wilks law gives the minimum umber of simulations that need to be run for a given sample's uncertainty to be estimated given a tolerance limit "a" and a confidence limit at that tolerance level "b". [28][29]

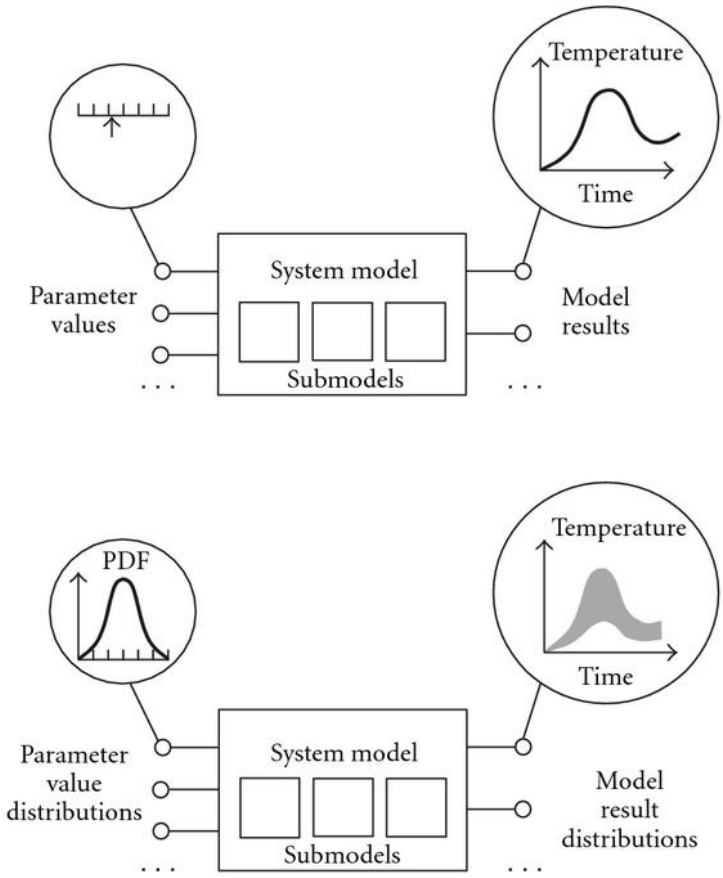

Fig. 5. Uncertainties from the relevant sources passed through the a sampling distribution [7]

The values are calculated from a simple formula given by:

$$1 - a^n \geq b \tag{6}$$

For a given distribution, it is then calculated that to estimate the uncertainty at a tolerance limit of 95 percent with a confidence level of 95 percent, 59 runs of surrogate CFD model is required with different samples of each of the input parameters. The number of runs for one-sided statistical distributions is given by the figure 6 as calculated by Glaeser for the GRS model. [7]

To construct the surrogate CFD model, random samples are generated in the uncertainty space defined by the uncertain input parameters. Each sample corresponds to a specific combination of input values. Sampling is done from a gaussian distribution

One-sided statistical tolerance limits			
b/a	0.90	0.95	0.99
0.90	22	45	230
0.95	29	59	299
0.99	44	90	459

Fig. 6. Minimum number of calculations required from the CFD model [7]

about a mean value and a standard deviation. The mean values are calculated from empirical correlations and the standard deviation is taken from a standard practice of 2.5. [30] These samples are then used to evaluate the CFD simulation model, generating a dataset of input-output pairs.

The results of the uncertainty quantification are presented in terms of probability distributions, statistical moments, and sensitivity rankings. The analysis provides insights into the impact of different input parameters on the output uncertainty and identifies dominant sources of uncertainty. Glaeser identified 56 parameters that effect peak cladding temperatures during blow down and re-flood condition in a reactor channel that effect channel design. A few included geometrical constraints, heat flux models and mechanistic material properties as shown in figure 7.

Several of these sources contribute to uncertainty in a wall boiling simulation as shown in 7 but most of them can be put aside with the scope of this work. The CFD model has a set CHF criterion defined by the RPI model[18] and the geometry has been defined as shown in sections below [31], leaving us with properties, or rather sources of uncertainty that arise from phase interaction with the wall and the bubble departure process as a direct consequence of the heat flux applied.

Hence a selection was made from the numerous wall boiling variables, with the selections being bubble departure frequency, bubble departure diameter, nucleation site density and boiling area fraction and UQ was established to investigate the effects of

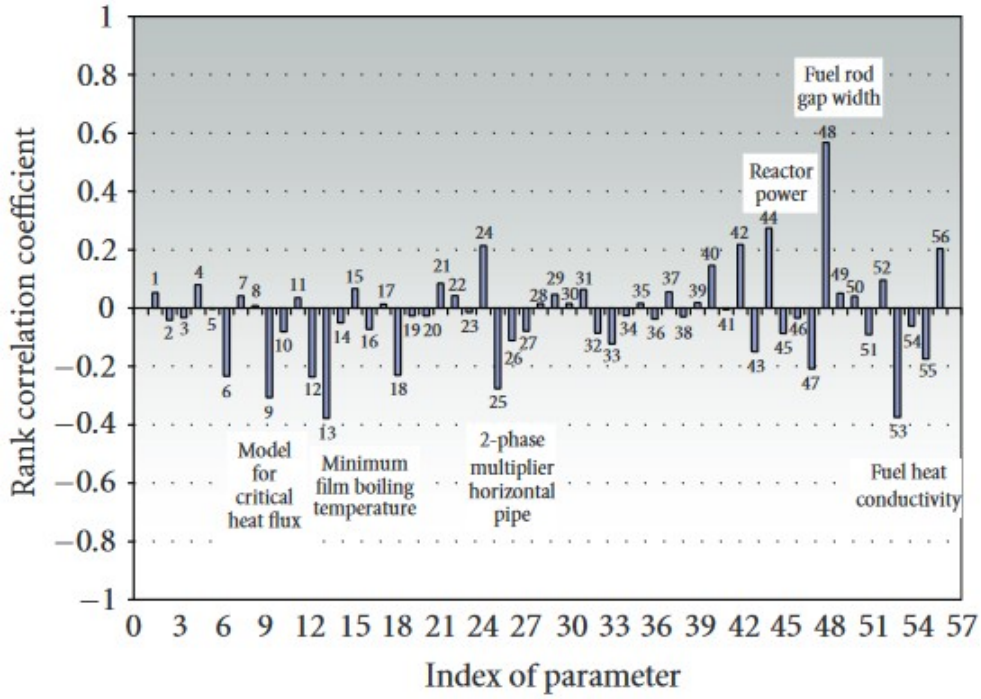

Fig. 7. Sensitivity measures of the peak cladding temperatures at blow down conditions with respect to the selected 56 uncertain input sources of uncertainty [7]

these parameters on the model.

For verification and validation of the mathematical output distribution of the surrogate model, a statistical test is needed for calculating the resemblance to an output ideal Gaussian distribution. Here the one sample Kolmogorov-Smirnov test is used that is devised to compare the ”empirical” cumulative distribution function (CDF) to the theoretical CDF as shown in figure 8. CDF is the probability of finding a variable value less than or greater than the value ’x’ in an iterative process. Hence the maximum value in the distribution has a CDF value of 1. The KS-test uses a null hypothesis that the data distribution or the empirical distribution is tested against of whether the data follows a Gaussian distribution or not. A k-statistic is used to measure the maximum distance or vertical difference between the CDFs as a test metric. This value should fall below a given critical value for a specified significance level, chosen to be a standard value of 5 percent [32]. The critical value for this significance level is given to be 0.175. If the k-statistic for the sampled distribution falls below this vale, the test is considered to be

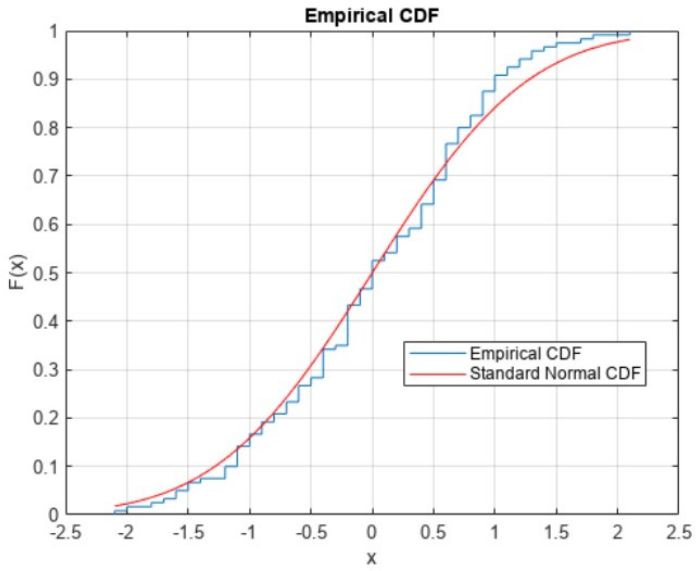

Fig. 8. Example for a fitness test comparison between empirical CDF and theoretical probability [32]

passed.

Sensitivity analysis is used to estimate the impact of the UQ parameters. Two correlational methods were deployed, Pearson [33] and Spearman's rank correlational coefficient method [34].

Pearson correlation coefficient is depicted as "r" that represents the statistical measure used to assess the linear relationship between two continuous variable. The range is from -1 to 1, with values closer to -1 implying a strong negative correlation and values near 1 representing a strong positive correlation. To assess the performance of CFD simulations for wall boiling in nuclear reactor fuel channels, the Pearson correlation coefficient has been applied. The mathematical formulation is given as:

$$r = \frac{\sum (X_i - \bar{X})(Y_i - \bar{Y})}{\sqrt{\sum (X_i - \bar{X})^2 \sum (Y_i - \bar{Y})^2}} \tag{7}$$

where X and Y are two different variables which undergo a correlation study.

Spearman's method differs slightly from Pearson's with the fact that it uses rank of the variable instead of the actual data. The method uses a rank system to assign and

sort the data, and to correlate the two variables. The rank of one variable, or one of the UQ parameters is then correlated against the rank of the other, or the maximum wall temperature to get a correlational coefficient 'ρ' for the two datasets of the variables. The mathematical formulation is given as:

$$\rho = 1 - \frac{6 \sum(\Delta \text{Rank}^2)}{n(n^2 - 1)} \tag{8}$$

Here ΔRank is the difference between the ranks of two corresponding data samples of the variables for which the correlation is being estimated. The rank of the variable is determined from sorting the dataset in order and assigning a rank based on the magnitude of the value. Pearson and spearman correlations have been used in a host of CFD methodology including the modelling of bubbly flows using multiphase models, which is representative of the case that we investigate here.[35]

2.4 Boiling Models

2.4.1 Bubble Departure Diameter

Kocamustafaogullari's model is a significant contribution to the field of two-phase flow, focusing on the prediction of bubble departure diameter. The model takes into account the effects of bubble shape, gas and liquid properties, and hydrodynamic conditions.[36] The departure diameter d_w is described by the following equation:

$$d_w = d_1 \cdot \theta \cdot \left(\frac{\sigma}{g \cdot \Delta p} \right)^{0.5} \cdot \left(\frac{\Delta p}{\rho_g} \right)^{0.9} \tag{9}$$

where,

- d_1 is a dimensionless constant.
- ρ_g and ρ_l are the densities of the gas and liquid phases, respectively.
- σ is the surface tension between the gas and liquid phases.
- $\Delta\rho$ is the density difference between the gas and liquid phases.
- g is gravity
- θ is the bubble contact angle

Several models have been proposed to predict bubble departure diameter, each with its own assumptions and limitations. When compared with these models, Kocamustafaogullari's model stands out due to its comprehensive approach that considers the effect of multiple parameters. The widely used Tomiyama model simplifies the prediction by focusing solely on hydrodynamic forces, neglecting the effects of fluid properties and surface tension. On the other hand, the other hand, models may take a more empirical approach by incorporating statistical analysis of experimental data. While these models have their merits, they may lack the adaptiveness and accuracy provided by Kocamustafaogullari's model.[37] Other models also exist which are derived from mechanistic formulations [38]or theoretical correlations that exist for specific cases and conditions in boiling.[39]

2.4.2 Bubble Departure Frequency

Bubble departure frequency is a critical parameter in the study of two-phase flow phenomena, particularly in boiling systems. Various models have been proposed to predict bubble departure frequency, and this section focuses on the model presented by Cole [40], along with a comparison to other existing models. The mathematical formulation of Cole's model for bubble departure frequency 'f' will be examined, and a detailed

analysis of its strengths and limitations will be provided.

$$f = \left(\frac{4g(\rho_{\mathrm{L}} - \rho_{\mathrm{G}})}{3d_w \rho_{\mathrm{L}}} \right)^{0.5} \tag{10}$$

where,

- g is gravity
- ρ_g and ρ_l are the densities of the gas and liquid phases, respectively.
- d_w represents bubble departure diameter

Cole's model incorporates nucleation site density and bubble growth rate as key factors affecting bubble departure frequency. The model's mathematical simplicity allows for quick estimations of departure frequency based on these parameters. However, the model assumes idealized conditions and neglects factors like bubble coalescence, which can be significant in dense bubble fields, and may not be able to accurately capture transient conditions.[41]

2.4.3 Nucleation Site Density

Ishii's model is rooted in statistical mechanics and makes use of the concept of critical cavities. The critical cavities are small groups of atoms or molecules with the minimum size necessary for stable nuclei formation. These clusters are characterized by their energy barriers for nucleation and their size distribution.[42] Ishii's model employs the following mathematical framework:

$$n" = n''_{\mathrm{avg}}(1 - e^{-\frac{\theta^2}{8\mu^2}})(e^{f(\rho^+)\lambda'/R_c} - 1) \tag{11}$$

Where:

- n" represents the nucleation site density at a specific location.
- n''_{avg} is the average cavity density.
- θ is a wall contact angle.
- μ is the wall contact angle scale.
- $f(\rho^+)$ is a function dependent on the density of the surrounding medium.
- λ' is a cavity length scale.
- R_c is the critical cavity radius.

This equation describes the nucleation site density n" as a function of various parameters, including θ, μ, ρ^+, λ', and R_c.[43] It incorporates terms related to the average cavity density and the wall contact angle, providing insights into how nucleation site density varies based on these factors. Since the cavity density varies at all locations across the model, an attempt will be made to vary the average cavity density for each of the surrogate models.

2.4.4 Bubble Influence Boiling area fraction

Understanding the distribution and coverage of vapor bubbles on a heated surface, known as the boiling area fraction A_b , is a critical aspect of investigating subcooled boiling phenomena. Over the years, several models have been developed to predict and analyze A_b, contributing to our comprehension of the complex interaction between fluid dynamics, heat transfer, and phase change during subcooled boiling. In this section, we

delve into the prominent boiling area fraction model proposed by Kurul and Podolski in 1990.[18]

$$A_b = F_a \cdot \frac{\pi \cdot d_w^2}{4} \cdot n'' \tag{12}$$

- F_a is the boiling area fraction
- n" is the average cavity density
- d_w represents bubble departure diameter

F_a represents the fraction of the surface area covered by bubbles. This parameter accounts for the spatial distribution and density of bubbles on the heated surface. The value of F_a varies from 0 to 1 in various conditions of boiling, with 1 being set at a criterion of critical heat flux when heat transfer is reduced due to complete coverage of the wall surface area by a blanket of vapour, and exceeds 1 in very violent conditions such as for models developed for very high pressure test cases.[2][43] Here however, we look at operations which approach CHF but do not meet them, hence a value of 0.9 has been given.

The Kurul and Podolski model offers an elegant approach to estimating boiling area fraction in subcooled boiling scenarios. Its formulation, which avoids the need for empirical constants, aligns well with the underlying physics of bubble coverage.

3 Methodology

3.1 Introduction

This section outlines the comprehensive methodology employed in the investigation of uncertainty quantification (UQ) for Computational Fluid Dynamics (CFD) predic-

tions of wall boiling within a nuclear reactor fuel channel. The objective of this study is to systematically analyse and propogate the uncertainties inherent in CFD simulations, providing a statistical approach for predictions of wall boiling phenomena. The methodology includes the following key steps:

- **Geometry Modelling and CFD Preprocessing** The investigation focuses on a typical nuclear reactor fuel channel, characterized by its geometry, material properties, and operating conditions. The reactor channel geometry is carefully defined based on available design specifications, encompassing the fuel rod assembly, coolant flow channels, and structural components. The material properties of the fuel rods, coolant, and structural materials are collected from validated sources. Operational parameters such as inlet velocity, pressure, and temperature are set to replicate real-world conditions.

- **CFD Modelling** A CFD model is developed using established software, in this work, using StarCCM+. The computational domain includes the fuel channel geometry and the surrounding fluid domain. The governing equations of fluid dynamics, including the Navier-Stokes equations, are discretized using appropriate numerical methods, with turbulence modeled using techniques such as Reynolds-Averaged Navier-Stokes (RANS) and the k-epsilon model. Boundary conditions are defined at the inlet, outlet, and walls of the domain, including proper treatment of phase change phenomena occurring at the wall.

- **Uncertainty Quantification** A comprehensive uncertainty characterization process is undertaken to identify and quantify various sources of uncertainty in the CFD simulations. These sources include input parameter uncertainties (e.g., material properties, boundary conditions), modeling uncertainties (e.g., turbulence models, phase change models), and numerical uncertainties (e.g., grid resolution,

time step) and a statistical standard is set to pursue UQ and propagate these sources through the CFD model.

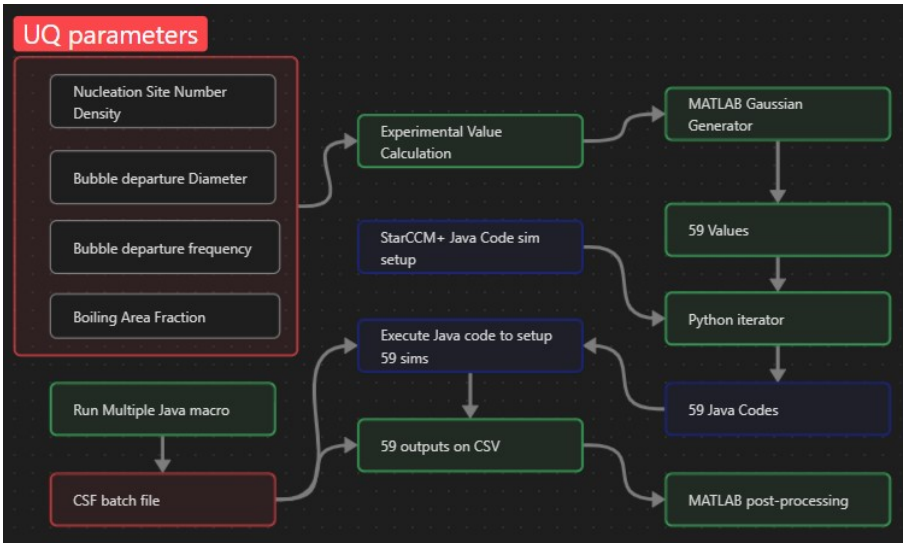

Fig. 9. Methodology followed for UQ of wall boiling in a nuclear reactor fuel channel

A multi-step method involving computational multi-fluid dynamics for two-phase flows and the subsequent uncertainty quantification using statistical tools has been put forward and explained in detail as seen in figure 9.

3.2 Preprocessing

The CFD preprocessing includes all the predefined, calculated inputs and continua that are used in the CFD modelling of the reactor channel.

3.2.1 Geometry

The target geometry model was a nuclear reactor model that satisfies the basic design requirements of operation and adheres to safety standards set by policy making organisations.

This geometry is modelled as a test heavy water reactor taking into reference standards set by the International Atomic Energy Agency (IAEA) for the Joint Comprehensive Plan of Action (JCPOA) for which multiple annexes exist in the public .[31] The standards and the subsequent reactor has been proposed for the Arak Modernization Project due to be implemented in Iran as a joint venture participated many nuclear energy organizations. The proposed reactor in question is the Arak heavy water research reactor, now renamed as Khondab Heavy Water Research Reactor (KHRR). The model was created on SolidWorks 2020 is a rudimentry replication of the reactor geometry thus specified.[44]

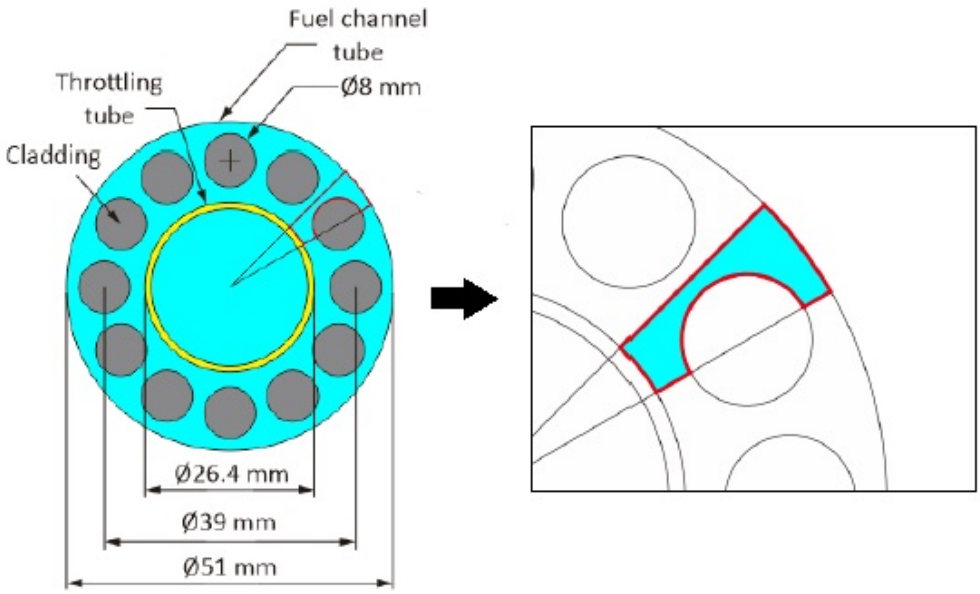

Fig. 10. Cross sectional view of reactor fuel channel

As seen in 10 the geometry has 12 fuel pins or channel tubes and a central throttling rod. The pins are surrounded by cladding material, specified to be Zirconium Alloys [31] which are 8mm in diameter. The pin assembly is encased in a 51 mm diamater fuel channel which forms part of the KHRR core where multiple channels of these kinds are put to use. Due to the axissymmetric nature of the geometry and for the purposes of modelling simplification, the reactor was then divided into 12 segments as shown in figures 10 and 11. The simplification was done on the computer aided design (CAD)

model itself and the surface mesh was imported to StarCCM+ using a STEP file.

3.2.2 Material Properties

The material properties used here in the simulation were directly taken from mathematical correlations that are specified in appendix A1. These correlations for the properties given in table 1 were a function of temperature ”T” used in celsius. Since the inlet temperature was 45 degrees celsius, that value was used to calculate all the properties for the liquid regime. The material properties for vapour were extrapolated from the starCCM+ documentation on wall boiling with the added assumption that heavy water [D_2O] is 10 percent heavier than normal water and the related properties are related as so. The saturation temperature was also calculated from a mathematical correlation,

Properties	Values
Heavy Water	
Density (kg/m3)	1095
Viscosity (Pa.s)	0.000714745
Thermal Conductivity (W/m.K)	0.632718
Specific Heat (J/kg.K)	4191.87
Vapour	
Density (kg/m3)	22.43
Viscosity (Pa.s)	1.78E-05
Thermal Conductivity (W/m.K)	0.0535
Specific Heat (J/kg.K)	4227.9

Table 1. Material Properties of fluid used in CFD modelling of wall boiling in the reactor channel

with a function dependent on pressure ”P”, which is used in megapascals. The absolute pressure of the system was 4.2 bara or 0.42 MPa, through which the saturation temperature was calculated to be 379.68 K. The calculation is shown in appendix A.

3.2.3 Boundary Conditions

The reactor sub-channel operates at a system pressure of 42000 Pa or 0.42 MPa which was set as reference pressure. Gravity also is applied to model buoyancy effects of the vapour phase by the natural convection phenomenon, set as a vector in the negative y-direction with a magnitude of 9.81 m/s^2.

The boundary conditions for the walls were applied directly on to the surfaces of the reactor sub-channel. There were three types of boundary conditions deployed, discussed below and shown in figure 11. Due to the axis-symmetric nature of the reactor sub-channel, three faces are given the symmetry boundary type, where a free-slip condition exists, assuming that the adjacent cell will have the same fluid flow characteristics outside the domain as on the cell on the wall. This type does not have any boundary layer on the mesh to resolve near wall behaviour.

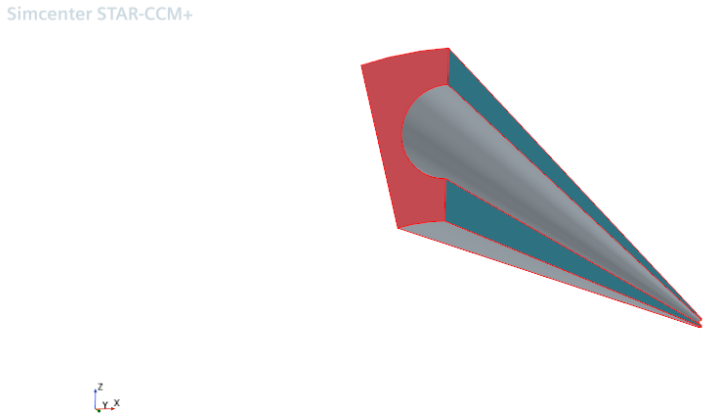

Fig. 11. Trimetric view of the reactor sub-channel with the boundary condition types shown in orange(inlet/outlet), cyan(symmetry) and grey(wall)

For the inlet, a velocity inlet condition was given with a field function specifying the inlet velocity as a vector. The inlet velocity was along the axis of the sub-channel with an inlet mass flux of 4719.53 kg/s divided by the liquid density of 1105 kg/m^3, resulting in an inlet velocity of 4.3 m/s. The input was given as the y-component of the

velocity vector. The vapour phase was given the same inlet conditions. The inlet was set at a temperature of 318.15 K or 45 degrees Celsius.

The outlet was specified as a pressure outlet with a gauge pressure of 0 Pa or 42000 Pa absolute pressure. The outlet temperature for the liquid phase was set at 331.15 K or 58 degrees celsius. The outlet temperature for the vapor phase is at saturation temperature.

The volume fractions for liquid phase was 1 and for the vapour phase was set to 0.

The wall towards the fuel rod cladding had a thermal heat flux specification applied. The wall was heated up to a ”critical” Hot Full Power (HFP) state in multiple iterations. It is the scenario in which the fission of nuclear materials produces a quantity of neutrons that is equal to or surpasses the nuclear containment’s capacity. In typical reactor functioning, nuclear fuel maintains a chain reaction of fission, known as criticality. Criticality in a reactor is reached when each fission occurrence releases an adequate number of neutrons to sustain a continuous sequence of reactions.[45] The heat flux applied was calculated from the fuel rod linear power rating. The linear power rating distribution is shown in figure 12 and the heat flux calculation is shown in appendix A.1.

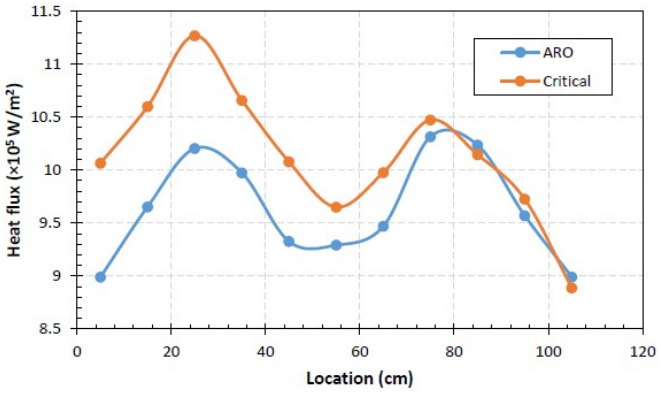

Fig. 12. Heat flux of ARO and critical heat transfer condition at the wall

3.2.4 Initial Conditions

The temperature within the liquid domain was setup as a constant temperature gradient between the inlet and the outlet boundaries ranging between 318.15 K and 331.15 K. The velocity in the entire domain for the two phases was kept as the inlet velocity vector of [0, 4.3 m/s , 0].

3.3 CFD Methodology

In the pursuit of developing a CFD model for predicting wall boiling in a nuclear reactor fuel channel, the criteria governing model selection are of paramount importance. These criteria revolve around four fundamental considerations. First and foremost, the selected CFD model must demonstrate a high degree of accuracy, as it must faithfully represent heat transfer and phase change phenomena within the fuel channel. Computational efficiency is equally crucial to ensure that the chosen model can perform simulations efficiently within available computational resources. Furthermore, the model's applicability to the specific geometric and boundary conditions of the fuel channel under investigation is a non-negotiable requirement. Within the segregated fluid temperature model, the governing equations of fluid flow, heat transfer, and mass transfer are solved simultaneously. The turbulent flow is characterized using a suitable turbulence model, accounting for the convective heat transfer and turbulence-induced mixing in the reactor core. Additionally, the model incorporates phase change mechanisms to simulate the nucleation, growth, and departure of vapor bubbles from the fuel rod surface.

Furthermore, a phase change model is incorporated to track the evolution of the vapor phase within the coolant, taking into account factors such as bubble nucleation, growth, and departure. The numerical scheme employed for discretizing the governing

equations is rigorously validated to ensure numerical stability and accuracy in capturing the complex phase change phenomena.

Lastly, the credibility of the model hinges on its ability to undergo successful validation against experimental data or established benchmarks, particularly for scenarios that bear similarity to boiling conditions. These selection criteria serve as the guiding principles for the systematic identification of the most suitable CFD model for our study, thereby ensuring its relevance and reliability in the context of nuclear reactor fuel channel analysis.

3.3.1 Fluid Flow Regime

The fundamental governing equations for simulating fluid flow and heat transfer are the Navier-Stokes equations. The incompressible form of these equations, considering conservation of mass and momentum, is used:

Continuity Equation

$$\nabla \cdot \mathbf{u} = 0 \tag{13}$$

Momentum Equation

$$\frac{\partial(\rho \mathbf{u})}{\partial t} + \nabla \cdot (\rho \mathbf{u}\mathbf{u}) = -\nabla p + \nabla \cdot \tau + \rho \mathbf{g} \tag{14}$$

Where u is the velocity vector, p is the pressure, ρ is the density, ν is the dynamic viscosity and f represents external forces like buoyancy. To capture the two-phase flow in the reactor fuel channel, the momentum equation is modified to account for the presence of both liquid and vapor phases. Key considerations include:

1. Interfacial Forces: The surface tension forces at the liquid-vapor interface are

incorporated into the momentum equation. These forces act to maintain the integrity of the liquid-vapor interface and influence the bubble dynamics.

2. Phase Interaction Terms: A volume fraction approach is used to track the local distribution of the two phases. The momentum equation includes terms that account for the volume fractions of both phases, allowing the model to distinguish between liquid and vapor regions.

3. Phase-Specific Properties: The density and viscosity of each phase are treated as phase-specific properties. This allows for variations in fluid properties between the liquid and vapor phases.

4. Bubble Dynamics: The momentum equation incorporates drag and lift forces on the bubbles. These forces arise due to the relative motion between the bubbles and the surrounding fluid and play a crucial role in predicting bubble behavior and distribution.

5. Turbulence Modeling: The presence of bubbles can significantly impact the turbulence characteristics of the flow. Turbulence models, such as the k-ε turbulence model, are coupled with the momentum equations to account for the effects of turbulence in the two-phase flow.

Energy Equation The energy equation accounts for heat transfer within the reactor fuel channel.

$$\frac{\partial(\rho E)}{\partial t} + \nabla \cdot (\rho E \mathbf{u}) = \nabla \cdot (\lambda \nabla T) + \rho \dot{q} \tag{15}$$

Where T is the temperature, c_p is the specific heat capacity, k is the thermal conductivity and q represents heat sources/sinks, including nuclear heating.

To accurately capture the energy transfer in a two-phase flow scenario with boiling, several considerations are essential:

1. Phase Change Phenomena: Latent Heat: The energy equation includes the latent heat term to account for the energy absorbed or released during phase change processes. When liquid turns into vapor (boiling), it absorbs latent heat, and when vapor condenses back into liquid, it releases latent heat. This term is critical for accurately modeling temperature variations during boiling and condensation.

2. Interfacial Heat Transfer: Boiling and Condensation Models: Appropriate models are incorporated into the energy equation to describe the heat transfer rates at the liquid-vapor interface. These models consider factors such as bubble growth, bubble departure, and the associated heat transfer rates.

3. Turbulence Effects: Turbulent Heat Transfer: In two-phase flow, turbulence can have a significant impact on heat transfer. Turbulence models, often coupled with the energy equation, account for the enhanced heat transfer associated with turbulent mixing in the presence of bubbles or droplets.

4. Heat Source Terms: Heat Sources and Sinks: The ”q” term in the energy equation accounts for any heat sources or sinks within the reactor fuel channel. This can include nuclear heating from fuel rods, frictional heating, or other localized heat generation mechanisms.

5. Wall Heat Transfer: Wall Boundary Conditions: The energy equation specifies appropriate wall boundary conditions to account for heat transfer between the fluid and the channel walls. These conditions should consider the phase change and boiling effects occurring at the wall.

To incorporate the considerations discussed above, additional closure relations and models are used to define the physics in the CFD modelling of the case.

3.3.2 Discretization

The finite volume method (FVM) implemented on Eulerian modelling in StarCCM+ is employed to discretize the governing equations on the grid. The discretized equations are solved iteratively using an implicit solver, with convergence criteria monitored to ensure solution stability. The cases investigated here showed a particular sensitivity to the turbulence model selection for both liquid and vapour phases and the particle size distribution model for the dispersed phase. They have been studied and discussed below as well.

3.3.3 Heat Transfer Regime

Boiling flow relations are linked to the Ranz-Marshall correlation [46], providing an empirical model for Nu. In terms of heat transfer, the Nusselt number measures the convective rate and is defined by the ratio of convective to conductive transfer across a boundary layer. The Ranz-Marshall correlation, proposed in 1952, provides an empirical expression for the Nusselt number (Nu) in boiling flows. It relates Nu to the Reynolds number (Re), Prandtl number (Pr), and a dimensionless factor, the Lewis number (Le). The correlation has been widely used due to its simplicity and reasonable accuracy in predicting Nu under a range of conditions. The correlation is typically expressed in StarCCM+ [43] as follows:

$$Nu = 2 + 0.6Re^{0.5}Pr^{0.3} \tag{16}$$

3.3.4 Turbulence Modelling

The k-epsilon turbulence model will be utilized to simulate the turbulent flow and heat transfer processes for the liquid flow regime in the RANS framework. The two additional models that are chosen are realizable k-epsilon two layer and two layer all y+ wall treatment on StarCCM+. The Navier-Stokes equations, which govern the fluid flow, are augmented with the energy equation and the k-epsilon turbulence model equations to describe the turbulent flow and heat transfer. The k-epsilon model involves two transport equations: one for turbulent kinetic energy (k) and another for the turbulent dissipation rate (ε). The equations are as given in the appendix as equation 28 and 29. The Two-Layer All y+ wall treatment is employed to accurately model the near-wall region where boiling occurs. This model accounts for the influence of wall proximity on turbulence and resolves the turbulent boundary layer from the viscous sub-layer to the fully turbulent region. Wall functions are applied in the near-wall region for efficient computation.

Issa's turbulence response model [47] is used to model the vapour phase or in this work, the dispersed phase in the wall boiling regime. This approach considers the turbulence exhibited by the dispersed phase as an empirical correlation to the turbulence present in the surrounding continuous fluid. It introduces a turbulence response coefficient (Ct) for bubbly flows, which quantifies the ratio between the velocity fluctuation of the dispersed particles and that of the continuous fluid phase. It is described as C_t. The turbulence response model proposed by Issa provides an estimation of the Ct value, which can reach up to 3 for extremely low volume fractions of dispersed phase. Nevertheless, this value swiftly diminishes to 1 when the volume fraction of the dispersed phase surpasses approximately 5 percent.[48]

3.3.5 Drag Force Modelling

The drag force experienced by vapor bubbles in a two-phase flow regime is a complex phenomenon dependent on various factors, including bubble size, shape, velocity, and local flow conditions. Several models have been proposed to predict these forces, and among them, the Contaminated Tomiyama Correlation has gained prominence due to its effectiveness in capturing the complex physics involved. The original Tomiyama Correlation, developed by Tomiyama et al. (1998) [49], was formulated for bubble diameter ranges up to 10 mm and accurately predicted the drag force in bubbly flows. However, the accuracy of this correlation diminishes when applied to sub-millimeter-sized bubbles, as encountered in boiling flows within nuclear reactor fuel channels. To address the limitations of the original Tomiyama Correlation, the Contaminated Tomiyama Correlation, introduced by Tomiyama et al (2002) [50], extends its applicability to microbubbles and contaminated bubble flows. This correlation considers the influence of contamination (non-condensable gases) on the drag force. In the context of nuclear reactor simulations, the presence of non-condensable gases (e.g., hydrogen) can significantly affect bubble dynamics and wall boiling behavior. The drag force F_{drag} on a single vapor bubble in a two-phase flow can be calculated as:

$$F_{\text{drag}} = \frac{4}{3}\pi R^2 \rho_l \left(1 - \frac{\rho_g}{\rho_l}\right) g + C_d \frac{1}{2} A_f \rho_l \left|U_r - U_b\right|^2 \tag{17}$$

where, R is the radius of the bubble, ρ_l is the density of the liquid phase, ρ_g is the density of the gas phase, g is the acceleration due to gravity, C_d is the drag coefficient, A_f is the reference area of the bubble (typically taken as the cross-sectional area), U_r is the relative velocity between the liquid phase and the bubble and U_b is the velocity of the bubble. In the Contaminated Tomiyama Correlation, the drag coefficient C_d is modified

to account for the presence of non-condensable gases. The modified drag coefficient is given by:

$$C_d = \frac{24}{Re}\left[1 + \frac{0.15}{\sqrt{Bo}} + 0.05Bo\right] \tag{18}$$

where, Re is the Reynolds number and Bo is the Bond number calculated as:

$$Re = \frac{\rho_l |U_r - U_b| R}{\mu_l} \tag{19}$$

$$Bo = \frac{\rho_l g R^2}{\sigma} \tag{20}$$

3.3.6 Particle Size Distribution

The S-Gamma particle size distribution model on starCCM+ aims to improve the accuracy of wall boiling predictions by accounting for a broader range of particle sizes and to account for bubble break up and coalescence in the dispersed phase of the regime.[51][52] The model is based on the two-parameter S-Gamma distribution function, which characterizes the distribution of particle sizes within the boiling flow. The parameters are the first and second moments of number density n(d_p, determining the number of particles and the interfacial area. [43] The S-Gamma model is particularly suitable for multiphase flows exhibiting a wide particle size range, such as the complex two-phase flow encountered in nuclear reactor fuel channels during boiling. The mathematical formulation is shown in the appendix as equation 30.

3.4 Uncertainty Quantification

As explained in literature above, the method for UQ adopted here is the Wilks non parametric GRS method that estimates the uncertainties of the model independently of the number of parameters and their significance as an input, only relying on their sampling and its distribution.[7]

Parameter	Correlation	Mean Value
Nucleation Site Density	Hibiki Ishii[48]	472000
Bubble Departure Diameter	Kocamustafaogullari[36]	0.000113133
Bubble Departure Frequency	Cole[40]	338.497
Boiling Area Fraction	Kurul Podolski[18]	0.004270248

Table 2. Calculated mean values for the parameters used in GRS uncertainty quantification

The sampling distribution taken here is a Gaussian distribution about a mean value that is calculated based on empirical correlations that exist in theory as discussed above. The values have been calculated in appendix A and are given as seen in table 2 with the correlations from which they have been calculated from.

The data set that was obtained was made from sampling from this the Gaussian distribution obtained around this mean value for a standard deviation of 2.5. The sampling was done on MATLAB and the distribution data set is given in appendix B.

The parameters have been used to estimate values for 95 percent confidence for a 95 percent tolerance limit, and using Wilks[28] law, 59 samples were taken from the gaussian distribution which have been shown for comparison in figure 13. These values are then checked for actual confidence estimates and are then exported for the surrogate model for UQ propagation.

The workflow for obtaining the CFD predictions and subsequent post-processing involves several key steps to efficiently set up and execute complex simulations using StarCCM+ as shown in figure 9.

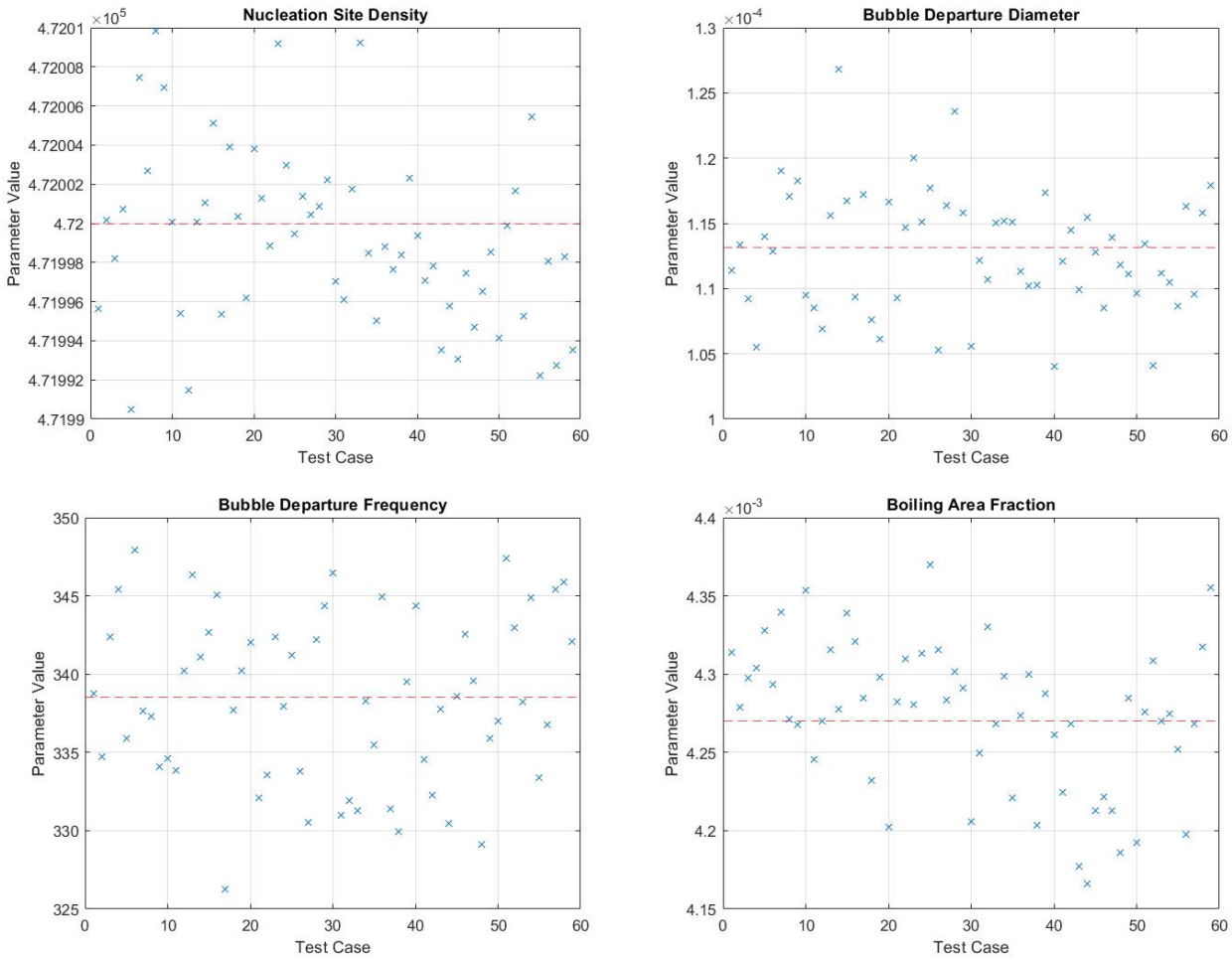

Fig. 13. UQ parameter samples for each of the 59 cases for UQ parameters, with mean value (dashed red line) taken for reference

Data Sampling and Preparation

We initiate our study by obtaining four distinct sampling datasets, which serve as essential inputs for our computational fluid dynamics (CFD) model. These datasets are instrumental in characterizing the different operating conditions within the reactor fuel channel.

Base CFD Model Setup

The foundational framework of our CFD model is established in StarCCM+. This primary model, referred to as the ”base case,” is configured independently of the sampling data. Within this setup, we employ relevant field functions to emulate the physical phenomena at play, such as wall heat flux and initial temperature gradients across the

flow domain.

Java Code Integration

The base case configuration is translated into a Java code file. This approach allows us to streamline the simulation setup process by bypassing direct interaction with the StarCCM+ graphical user interface (GUI). Java serves as the source code for StarCCM+, enabling us to create a macro that imports a volume mesh file and proceeds to set up the entire simulation automatically.

Parameterization and Iteration

To accommodate the diverse scenarios represented by the sampling data, we parameterize the Java code. Initially, specific parameter values are embedded directly into the code. These values are subsequently replaced with variables designed for identifying the variable changes needed for each case.

Python Integration for Automation

A Python script is employed to read the Java code as a string within a Python environment. This script identifies the designated variables within the Java code. The Python script then iterates through the 59 cases discussed earlier, replacing these variables with actual values extracted from the sampling dataset. This iterative process generates 59 distinct Java codes, each tailored to a specific case, and these are stored under unique file names, each corresponding to its respective case number.

Batch Execution

To efficiently execute all the saved simulations within a designated folder, we utilize a Java executable batch file. This batch file is executed with the assistance of a bash job script, ensuring that the simulations run consecutively and without interruption.

Post Processing Lastly, all the data from the simulations is collected from the Star-CCM+ reports by implementing a similar workflow to run a macro that creates a CSV file, which is then processed through MATLAB for the KS test and the sensitivity analysis. MATLAB has been used as a post-processing tool due to its modular environment and the added advantage of inbuilt libraries for data processing and management.[32]

This comprehensive workflow enables us to conduct a thorough investigation into wall boiling phenomena in nuclear reactor fuel channels while optimizing efficiency and data management throughout the simulation process.

For the workflow concerning the UQ analysis, the GRS method was implemented.[7] Employing the Glaeser (2008) method in CFD predictions enables accuracy assessment and quantification of wall boiling uncertainties in fuel channel. Effective in tackling complex thermal-hydraulic simulations, this method has been widely recognized.

3.2.1 Input Uncertainties Starting with the identification of input uncertainties, the Glaeser method unfolds. Within the bounds of this investigation, parameters such as initial conditions, boundaries, materials, and turbulence modeling constants give rise to input uncertainties. Large swings in wall boiling behavior can arise from uncertainties.

3.2.2 Uncertainty Propagation Through the CFD model, how input uncertainties influence output predictions by probing uncertainty propagation. A simulation technique, Monte Carlo draws a large number of random samples from probability distributions to account for uncertain input parameters. Inputting each sample, the model then produces the resulting predictions.

3.2.3 Sensitivity Analysis Analyzing which input variables have the biggest effect on CFD forecasts, sensitivity evaluation is critical. To quantify the input uncertainties, metrics like Sobol indices are calculated.

3.2.4 Uncertainty Quantification From the Monte Carlo simulations, statistical analysis of the CFD results yields the uncertainty quantification. PDFs and confidence intervals are built for important output variables including wall temperature, heat transfer coefficients, and void fraction. Through these findings, we learn about the vast array of possible outcomes and their linked probabilities.

4 Verification and Validation

In order to establish the mesh independence of the simulation results, a comprehensive mesh sensitivity analysis was undertaken. To investigate the sensitivity of the simulation results to mesh resolution, we will primarily focus on varying the element size while keeping other mesh parameters constant. Element size is a critical factor that can significantly influence the accuracy and computational efficiency of CFD simulations.[30]

4.1 Mesh Refinement

Coarse Mesh

In the initial phase of the mesh sensitivity analysis, a coarse mesh will be generated with a relatively large element size. The purpose of this coarse mesh is to provide a baseline simulation. The element size for this mesh configuration will be set conservatively to reduce computational demands, but it may not capture fine details of the flow and boiling phenomena effectively. Typically, the coarse mesh element size will be chosen to be several times larger than the expected boundary layer thickness and characteristic flow features within the nuclear reactor fuel channel.

Medium Mesh

The medium mesh will serve as an intermediate step between the coarse and fine meshes. For this configuration, the element size will be refined compared to the coarse mesh. The aim is to strike a balance between computational efficiency and accuracy. Element size adjustments will be made to ensure that critical flow features and boiling regions are better resolved.

Fine Mesh

In the final phase of the mesh sensitivity analysis, a fine mesh will be generated with a significantly smaller element size. This mesh will aim to capture fine-scale details of the flow, boundary layer, and boiling phenomenon with higher fidelity. The element size for this mesh will be chosen to be smaller than or on the order of the expected boundary layer thickness. The fine mesh will require more computational resources but is expected to provide the most accurate representation of the wall boiling process.

4.2 Mesh Setting

During the mesh sensitivity analysis, mesh quality will be monitored and evaluated using appropriate metrics, such as aspect ratio, skewness, and orthogonality. Mesh quality checks will ensure that the variations in element size do not introduce poor-quality elements that could adversely affect simulation accuracy and stability. The assessment was done for each of the mesh and appropriate settings were chosen for the mesh study that are given in table 3. This detailed elaboration on the variation of element size in the mesh sensitivity analysis emphasizes its importance in assessing the impact of mesh resolution on CFD predictions of wall boiling in a nuclear reactor fuel channel. The respective mesh refinement is seen in figure 14 to visualize the difference in the settings

Directed mesh	Coarse (M1)	Medium (M2)	Fine (M3)
Base size	0.6mm	0.3mm	0.2 mm
Number of prism layer	3	3	3
Prism layer total thickness	0.6mm	0.15	0.1
Prism layer near wall thickness	0.12mm	0.031mm	0.021mm
Total number of cells	26072	93142	204242
Target y+	>40	5-10	<5

Table 3. Mesh settings for mesh dependency test

and the simulation was executed with identical conditions applied. A few of the field

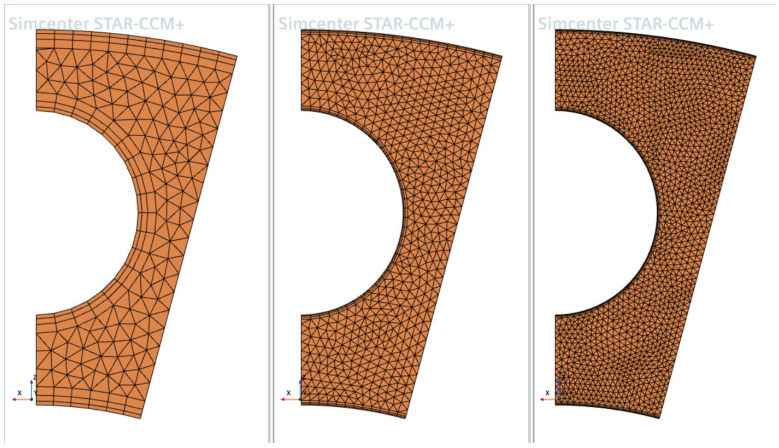

Fig. 14. Mesh scenes for three degrees of refinement for mesh dependency of the case

parameters were then compared to observe any changes in flow regime behaviour due to differing capture of flow phenomena, like the length scales in turbulence and volume fraction of vapour capture, that affect the fluid domain extensively. This behaviour is shown in figures 15 and 16 where boundary layers show are captured more effectively and are averaged to lesser extent in the domain. The results for the three mesh refine-

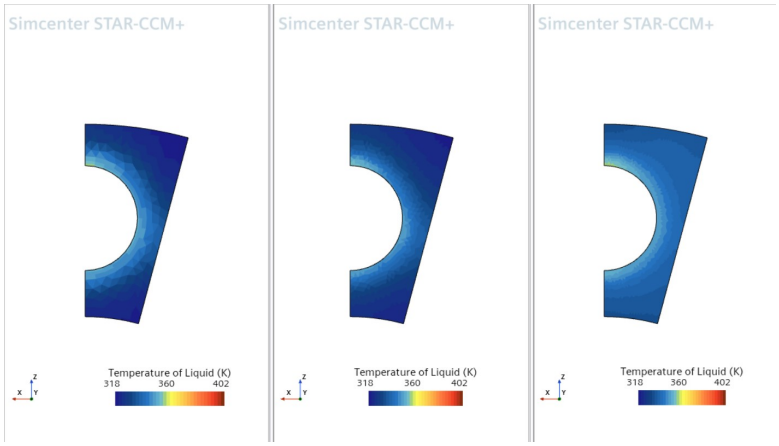

Fig. 15. Temperature of Liquid contour plot for mesh dependency test

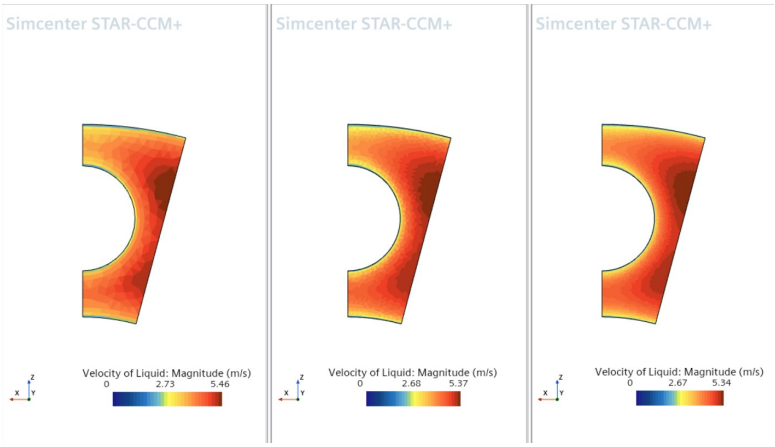

Fig. 16. Velocity Magnitude contour plots for mesh dependency test

Directed mesh	Coarse (M1)	Medium (M2)	Fine (M3)
Maximum Temperature of Liquid Coolant	401.632	401.83	402.06
Maximum Velocity Magnitude of Liquid	5.46	5.369	5.339
Wall Y+	44.83	9.197	4.601

Table 4. Results of mesh sensitivity test simulations

ment simulations are shown in table 4. Given these results, a rudimentary observation shows that the temperature and the velocity are observed to have a smaller difference in prediction between the medium and finer meshes M2 and M3. Though M1 broadly shows a good relationship to he results shown, the difference as compared to M2 and M3 is considerable, especially with velocity, which can be attributed to better vapour interface capture and to buoyancy effects of the vapour that contribute to increase in momentum of the liquid. This is also reinforced by the fact that phasic turbulence and phase coupled fluid energy models have been used in modelling these cases.[43] Hence mesh M2 was chosen for the UQ and a suitable basis for sensitivity analysis.

The results were also compared with Rahman's work [30] on similar geometry and conditions for the reactor but on a single phase simulation. The results seem to show a general agreement with the trends seen with an error of approximately 3.71 percent, attributed to the better heat transfer process captured in this work due to concise modelling of the vapour phase and differences in numerical modelling in StarCCM+.[43] A comparison was also done against experimental data obtained as a standard for JCPOA

regulations with the volume average coolant temperature (for the region with the heat flux) calculated for the critical condition to be 325.97 K from the simulation compared against a value of 324.85 K for the hot full power state as seen in table 8 giving an error of approximately 0.34 percent.[31]

5 Results and discussion

5.1 CFD Test Case Simulations

In this section, we delve into the post-processing of our verified model, incorporating both all rods out (ARO) and critical conditions. This approach has yielded diverse computational fluid dynamics (CFD) predictions that warrant a comprehensive comparative assessment. We have extracted a range of critical parameters from these simulations, encompassing fluid and wall temperatures, velocity profiles, and pressure drop characteristics. Given the overarching objective of our investigation, which centers on the evaluation of nuclear reactor safety, our study is particularly focused on two key aspects: the prediction of fluid temperature and the determination of maximum wall temperature within the fuel channel, each of which plays a pivotal role in understanding the safety margins and operational conditions of the reactor.

We see a sharp increase in temperature and volume fraction in figures 17 and 18 as the incoming fluid heats up across the length of the channel. Moreover,figure 17 offer valuable insights into temperature profiles at distinct elevations, corresponding to the All Rods Out (ARO) and critical heat transfer conditions, respectively. Remarkably, both conditions exhibit a strikingly analogous temperature distribution trend across all designated locations. Specifically, at the lower elevation of 0.3 meters, we observe

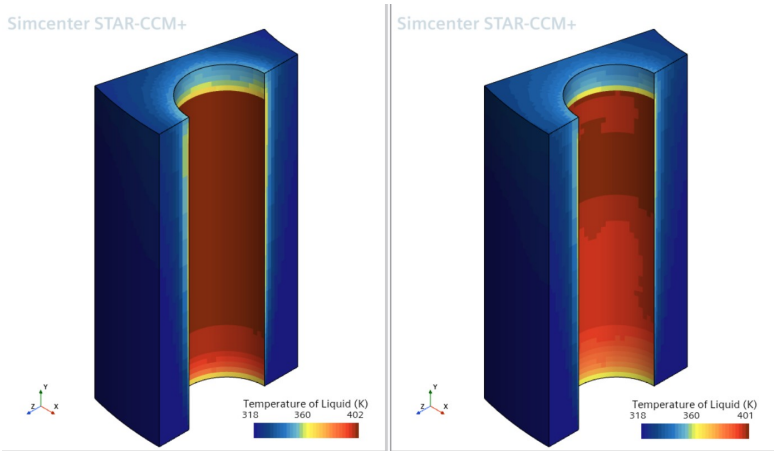

Fig. 17. Temperature of coolant contour plot of the base cases at critical and ARO conditions

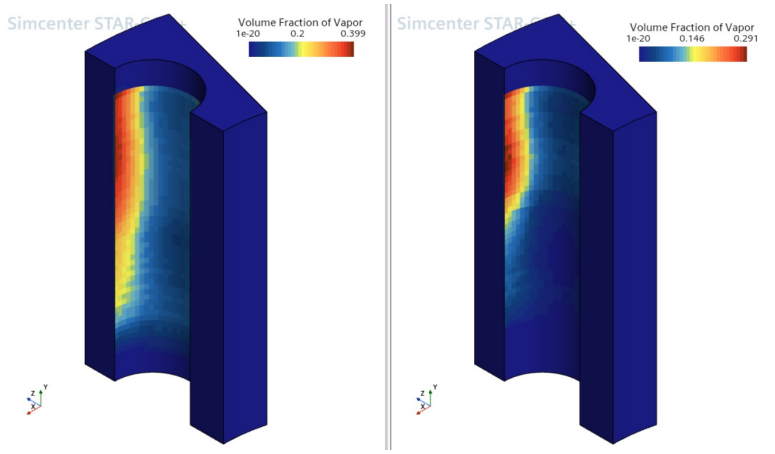

Fig. 18. Volume Fraction contour plot of the base cases at critical and ARO conditions

a we observe only minor fluctuations in fluid temperature across the cross-sectional area. However, as the elevation increases, the influence of heat transfer becomes more pronounced throughout the region, leading to a notably diverse distribution of fluid temperature as seen in 20. This observed phenomenon underscores the consistent behavior of temperature trends in our CFD predictions, underscoring the relevance of our uncertainty quantification efforts in the context of boiling within the nuclear reactor fuel channel. We also observe a small difference between the velocity of liquid between the two conditions as shown in figure 19, due to the increased buoyancy effects in the critical case. Figures 22 and 21 provide a visual representation of the wall temperature dynamics within the fuel channel, revealing a distinctive non-linear pattern. Notably, this temperature trend exhibits a sharp initial ascent from the inlet, extending

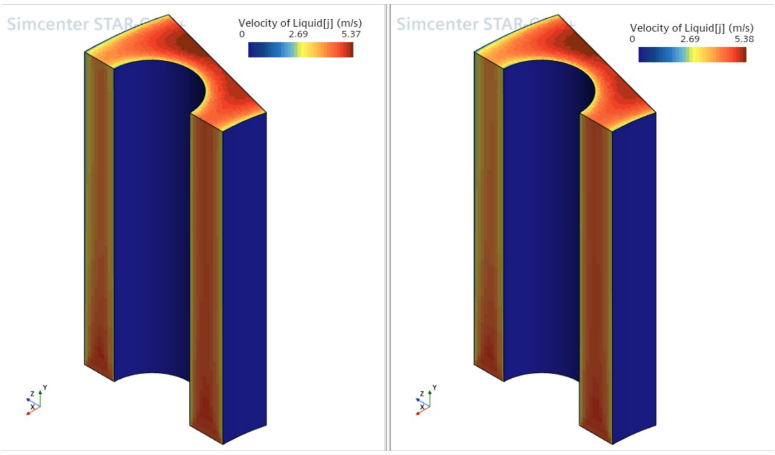

Fig. 19. Axial Velocity magnitude contour plot of the base cases at critical and ARO conditions

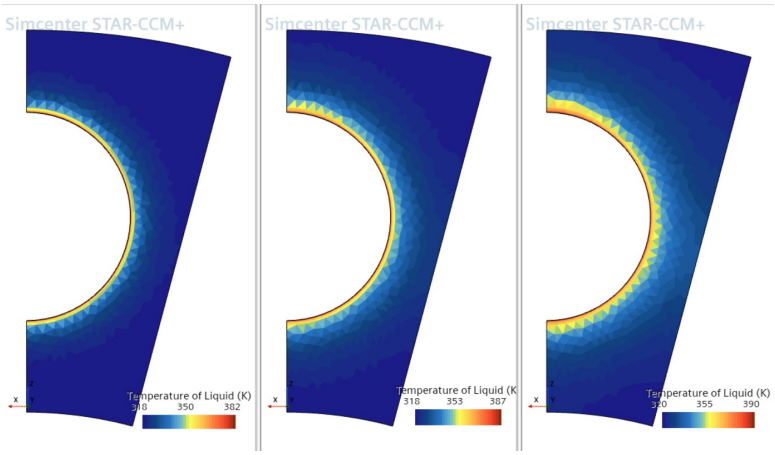

Fig. 20. Liquid temperature contour plot of the base cases at critical and ARO conditions across cross sectional area

up to 0.1 meters downstream, followed by a more gradual increase towards the outlet. This intriguing non-linear behavior can be attributed to the intricacies of the heat transfer process. It is crucial to acknowledge that the heat transfer rate, a critical factor in this context, is substantially influenced by a multitude of conditions, including but not limited to fluid temperature, velocity, density, and various other flow parameters.

5.2 Uncertainty Quantification

From the surrogate CFD model, following the GRS model and Wilks law, maximum wall temperatures were obtained for 59 cases from inputs with 95 percent confidence levels at 95 percent tolerance limits as shown in figure 23.

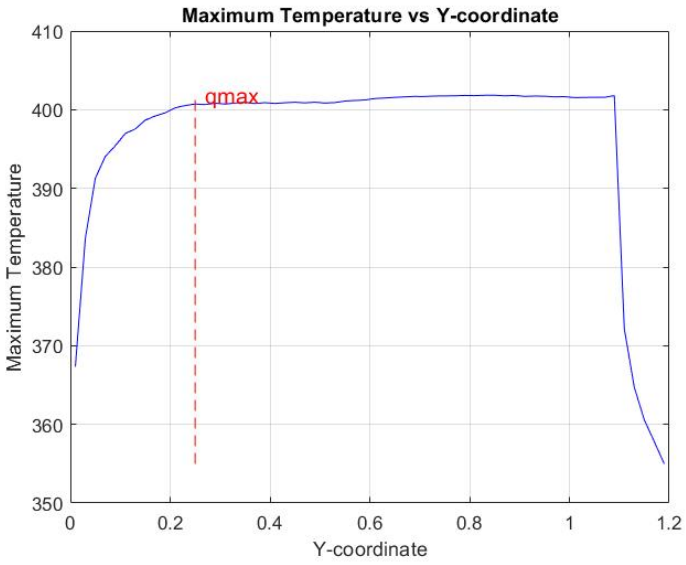

Fig. 21. Maximum temperature in the reactor sub channel for critical condition with position of maximum heat flux plotted for reference

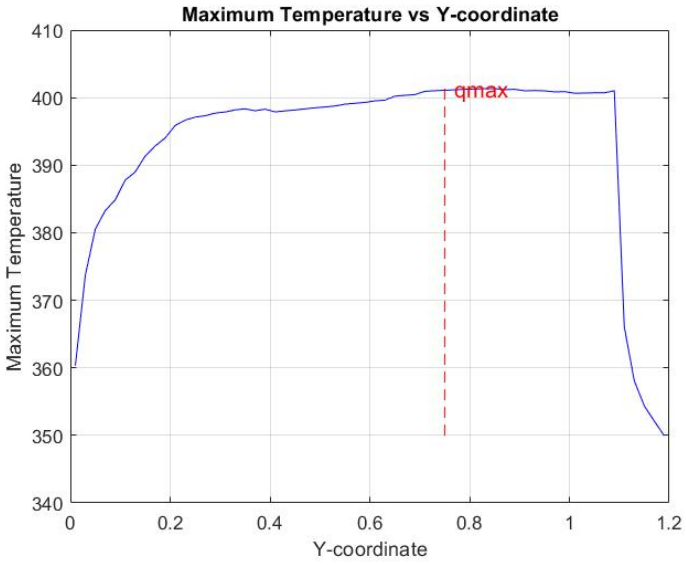

Fig. 22. Maximum temperature in the reactor sub channel for ARO condition with position of maximum heat flux plotted for reference

The K-S test that was conducted yielded a K-S statistic of approximately 0.1532 for the critical case and 0.1199 for the ARO case was calculated on MATLAB where the maximum vertical distance between the output sample and the theoretical Gaussian CDF. For a significance value of 5 percent the value for comparison was 0.1737 on MATLAB that was clearly greater than the calculated K-S statistic. Hence the K-S test for the output was cleared and a null hypothesis of the output data following a Gaussian distribution was proved to be true. The CDF of maximum wall temperature

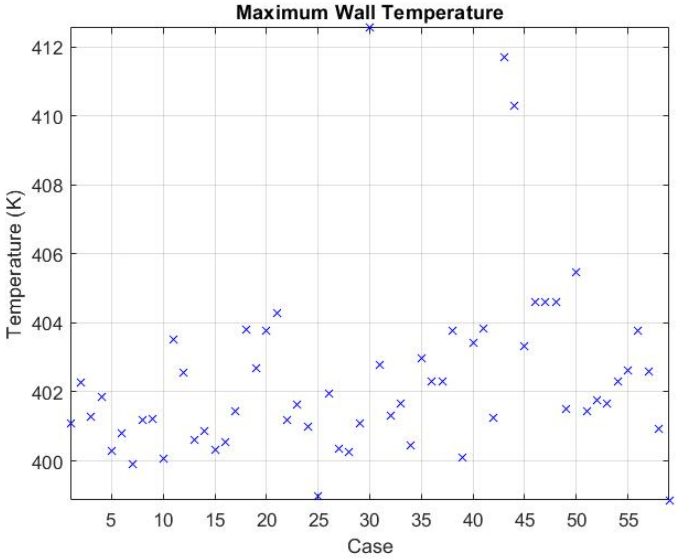

Fig. 23. Maximum wall temperature for the UQ cases with critical conditions

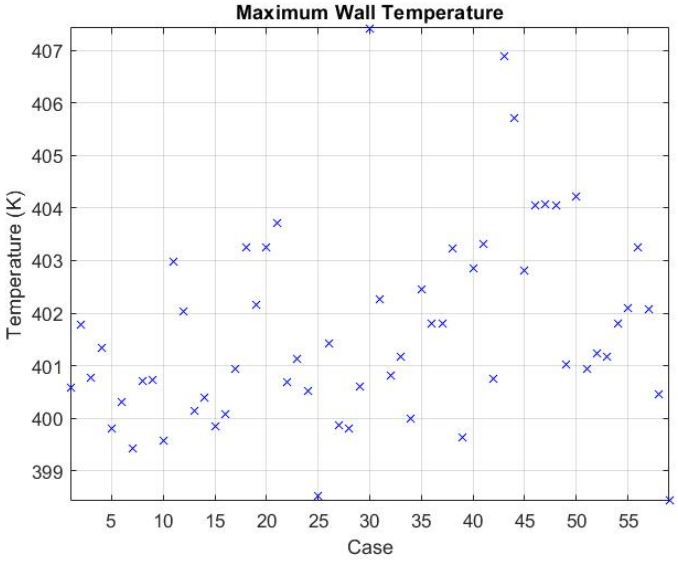

Fig. 24. Maximum wall temperature for the UQ cases with ARO conditions

for comparison against the Gaussian CDF for a mean max wall temperature value is shown in figure 25.

The mean and standard deviation output values from CFD models was also calculated to develop the theoretical Gaussian distribution for the KS test above. The mean value for the critical case was calculated to be a value of 402.3975 K and the standard deviation $\sigma_{T_{max}}$ was 2.5901 K. Following the GRS method for UQ [7], we find that the estimated upper limit for the maximum wall temperature at a 95 percent confidence

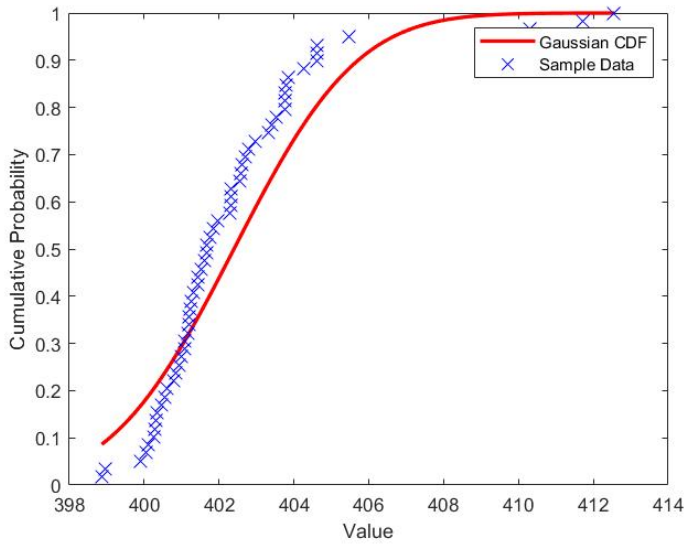

Fig. 25. KS fitness test comparison between empirical CDF and theoretical CDF for critical condition

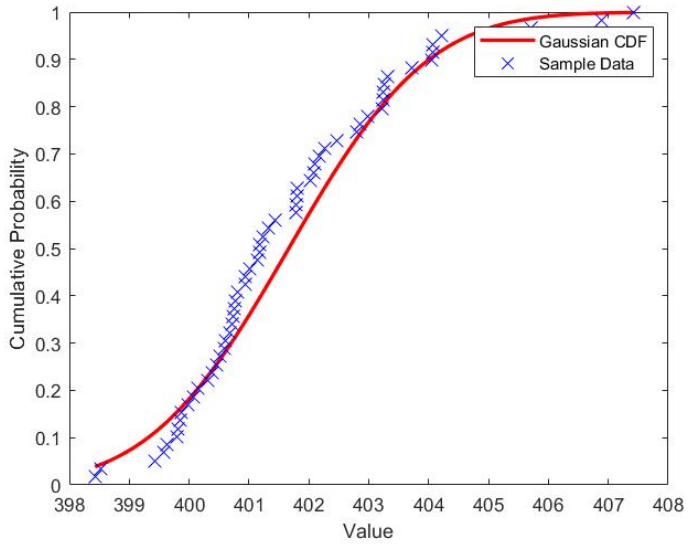

Fig. 26. KS fitness test comparison between empirical CDF and theoretical CDF for ARO condition

level would be then given as:

$$T_{max} = T_{mean} + 1.96 * \sigma \tag{21}$$

$$T_{max} = 402.3975 + 5.0784K \tag{22}$$

Similarly, for the ARO case, the mean value was calculated to be a value of 401.6631

K and the standard deviation $\sigma_{T_{max}}$ was 1.8313 K.

$$T_{max} = 401.6631 + 3.5893K \tag{23}$$

5.3 Sensitivity Analysis

As discussed before, the correlations used for sensitivity analysis are the Pearson and the Spearman methods of correlations that differ in using the actual data or the ranks of the correlation thus obtained. Both results give a monotonic relationship between the input and the output datasets and are very similar in their final interpretation. The sensitivity analysis was done on Maximum wall temperature with respect to the four UQ parameters: nucleation site density, bubble departure diameter, bubble departure frequency and boiling area fraction with the correlation shown for each output value in figures 27 and 28. The correlations for Spearman method have been given in the appendix D for reference as well.

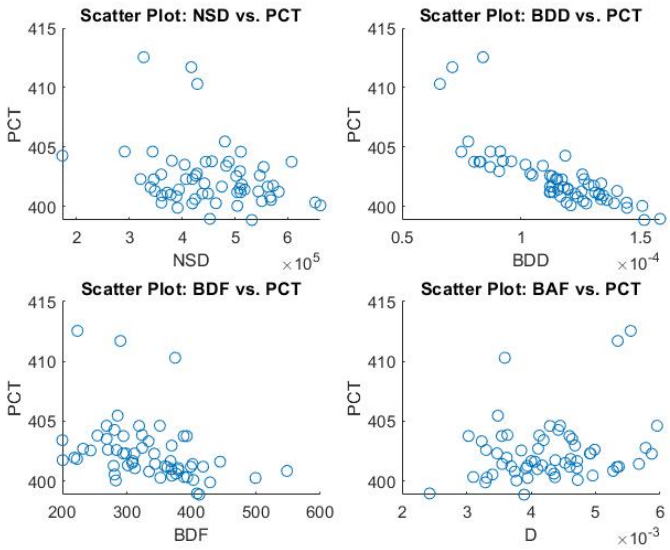

Fig. 27. Pearson Correlation plot between the UQ parameters and peak cladding temperatures for critical condition

On observation from the graphs, the near linear relationship for bubble departure

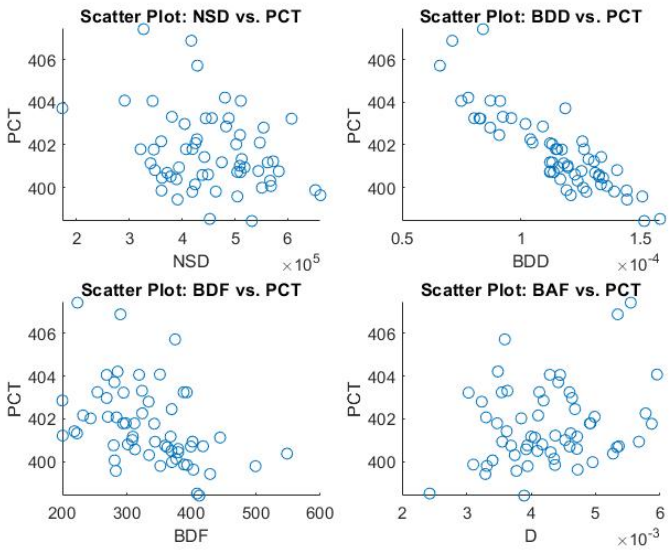

Fig. 28. Pearson Correlation plot between the UQ parameters and peak cladding temperatures for ARO condition

diameter shows that it has the maximum impact or sensitivity on the results of the simulation, corroborated by the figure 29 shown for a comparison of the coefficients and correlations used for sensitivity analysis. The actual values are shown in table 14 in Appendix C. The results from the sensitivity analyis are interpreted from a set quan-

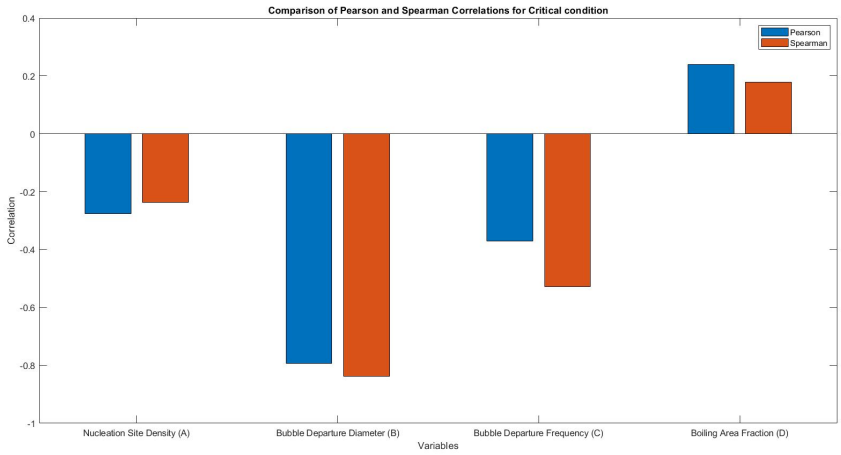

Fig. 29. Comparison between Pearson and Spearman correlational values for sensitivity analysis for UQ for critical condition

tifier explained in previous works [30], and the following ”standard” of observations exists in table 5. On observation from table 5 and on comparison with the sensitivity analysis results, we obtain that there is a stark difference between the sensitivity of the parameters towards the uncertain output data. Bubble departure diameter is the param-

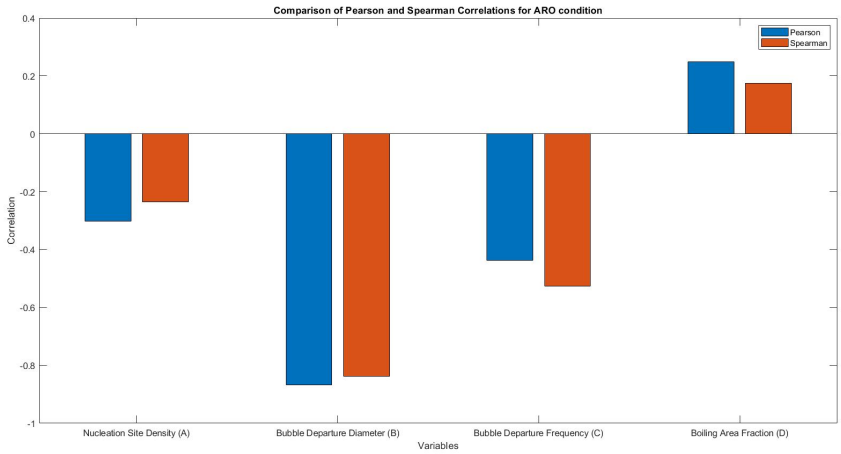

Fig. 30. Comparison between Pearson and Spearman correlational values for sensitivity analysis for UQ for ARO condition

Correlation constant	Classification
0	No relationship
0<|r|<0.19	No or negligible relationship
0.2<|r| <0.29	Weak relationship
0.3<|r| <0.39	Moderate relationship
0.4<|r| <0.69	Strong relationship
0.7<|r|	Very strong relationship

Table 5. Standards for interpreting correlational coefficients from sensitivity analysis

eter with the strongest sensitivity or impact on the maximum wall temperature in the model displaying values of magnitude above 0.7 showing a very strong relationship with the output. All the parameters show a negative sensitivity towards the maximum wall temperature except boiling area fraction, meaning as they increase the maximum wall temperature should decrease. In the mean time, nucleation site density and boiling area fraction showed a weak relationship with opposite magnitudes towards the estimation and bubble departure frequency showed a moderate relationship. It should be noted that the sensitivity measured here, depends on the physical significance of the mean values chosen for the analysis. A particular example is bubble influence boiling area fraction, where as stated above, the value chosen for the case was less than one, as we approach CHF conditions but do not meet them. A case with a higher boiling fraction area would still result in worse heat transfer rate giving rise to a positive sensi-

tivity. If the CHF criterion would have been met, the mean value chosen for boiling area fraction would have been one, or as seen in documentation [43] can exceed one, results in a similar positive sensitivity as a higher fraction with an already existing blanket of vapour would result in higher temperatures and even lower heat transfer rates.[30]

The same cannot be said for the other three UQ parameters as nucleation site density and departure frequency help in the formation of more bubbles that evacuate the heated wall of heat flux and the departure diameter helps in entrapment of more heat due to the surface tension of holding the bubble back from departure for an extended period of time.

In summary, this chapter's results provide a solid foundation for understanding the intricate processes governing wall boiling in a nuclear reactor fuel channel. The knowledge gained here is essential for reactor safety, performance optimization, and fuel rod design. Several key observations are drawn from the results presented in this chapter:

Boiling Phenomena Analysis: The CFD simulations have effectively captured the intricate boiling behavior near the fuel cladding surface. We have observed the formation and dynamics of vapor bubbles, bubble departure frequency, and the subsequent impact on heat transfer.

Heat Transfer Enhancement: By analyzing the local heat transfer coefficients, we have identified regions of enhanced heat transfer associated with boiling. These findings are crucial for optimizing fuel rod designs to improve thermal performance while maintaining safety margins.

Flow and Temperature Profiles: The velocity and temperature profiles obtained from the simulations offer valuable insights into the flow distribution and thermal stratification within the fuel channel. This information is essential for reactor safety analysis.

6 Conclusions

In conclusion, this work has endeavored to address the critical issue of uncertainty prediction in the context of Computational Fluid Dynamics (CFD) simulations for wall boiling in nuclear reactor fuel channels. The nuclear industry relies heavily on accurate predictions of heat transfer and boiling phenomena within these channels to ensure the safe and efficient operation of nuclear reactors. However, the inherent complexities of two-phase flow and the presence of uncertainty in model parameters make this task particularly challenging.

Each individual model underwent a subjective verification and validation processes, which included mesh sensitivity analysis, comparison to previous studies, and the utilization of experimental data. Following the successful validation of these models, an uncertainty quantification study was conducted by introducing uncertain parameters. Subsequently, statistical methodologies namely, the GRS method and the KS fitness test were employed to estimate the uppermost limit of the maximum wall temperature. Lastly, a sensitivity study of the temperature perdictions was done with respect to the UQ parameters which were nucleation site density, bubble departure diameter, bubble departure frequency and bubble influence boiling area fraction

The results indicate that uncertainty in CFD predictions can vary significantly based on the choice of turbulence model, boiling model, and heat transfer correlation, underscoring the need for careful model selection and calibration. The final uncertainty estimation for a nuclear reactor operating at critical condition was that the maximum wall temperature in the reactor sub-channel was 402.3975 K with an uncertainty of 5.0765 K; and for the ARO case, 401.6631 K with an uncertainty of 3.5893 K.

In both test cases, both the Pearson and Spearman correlation coefficients concur

in indicating that the bubble departure diameter is the most sensitive to uncertainty of maximum wall temperature, displaying a correlation coefficient of nearly -0.7 in the analysis. Subsequently, nucleation site density and boiling area fraction exhibit weak relationships with uncertainty, while the relationship between bubble departure frequency and uncertainty is deemed moderate.

7 Future Work

7.1 Interface Molecular Tracking

Interface tracking using methods like Volume Of Fluid (VOF) on a high fidelity simulation is a viable option given that more computational resources will be consumed. VOF can be implemented on StarCCM+ instead of the Eulerian Multiphase (EMP) model discussed above, reducing the errors and approximations brought about for bubble coalescence, breakup and departure by models like s-gamma and solution interpolation, so that each bubble, can be tracked, for smaller geometry or for macroscopic models and extrapolated to reproduce the entire reactor channel geometry. Firstly, it enables an accurate representation of the interface between different phases, allowing for precise modelling of the liquid-vapor interface as bubbles form and detach from heated surfaces. This accuracy extends to the simulation of bubble dynamics, as the software can track individual bubble movement, growth, deformation, and interactions. This dynamic understanding is crucial in boiling scenarios where heat transfer mechanisms are intricate due to phase changes. Interface tracking provides a detailed analysis of local phenomena like thin liquid film formation around bubbles and liquid entrainment by bubbles. This is significant in understanding complex interactions between liquid and vapor phases occurring on the channel surface. The technique also accounts for sur-

face interactions by modelling contact angles and surface wetting, influencing bubble behaviour and heat transfer. The inherent advantage here is that transient behaviour is captured as well as UQ due to discretization and rounding errors is reduced.

7.2 Alternate CFD Methods

Smoothed particle hydrodynamics (SPH) and lattice Boltzmann method (LBM) are two fluid dynamics (CFD) techniques that can be utilized to simulate wall boiling. SPH follows an approach whereas LBM follows an approach. SPH is particularly advantageous when it comes to simulating flows with moving boundaries whereas LBM is well suited for simulating flows, with high Reynolds numbers.

Implementing SPH is relatively straightforward. Allows for the simulation of large scale problems. It also captures the physics of small scale phenomena like the formation of vapor bubbles. However it's worth noting that SPH generally exhibits accuracy compared to LBM. LBM boasts efficiency. Lends itself well to simulating very large problems. It also captures the intricacies of multiphase flows. Nonetheless it should be acknowledged that LBM requires resources than SPH and can be slightly more challenging to implement.

Choosing the method depends on the problem at hand. If the flow is relatively slow and involves moving boundaries that are observed with microscopic scale boiling models, then utilizing SPH would be a choice. On the hand if there's turbulence in the flow, with a high Reynolds number then employing LBM would be a suitable option.

7.3 Machine Learning and Neural Networks

An outlook for further research could be the implementation of machine learning and physics informed neural networks to perform estimation of useful output parameters, using objective functions, quite like theoretical correlations used in the models used above. Some work in this spectrum has already been done for optimizing conditions to achieve maximum heat transfer for a given set of geometrical constraints, with the trained algorithm using parameters available as before and as shown in figure 31 .[53]

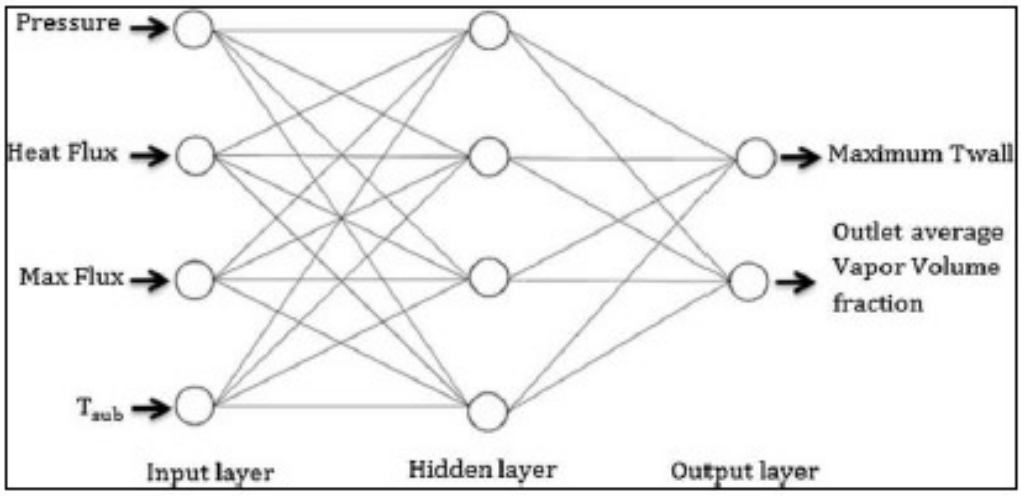

Fig. 31. Neural network to estimate maximum wall temperature using objective functions with the same input parameters as CMFD. [53]

Using these algorithms supplements the methodology examined for the purposes of this work, wherein redundant use of CMFD simulations is decreased with simultaneous in increase in computational load in the CMFD simulation. Instead, an algorithm can be trained to predict flow parameters for changing geometrical constraints as well as any material change for the same operating conditions without having to spend computational resources in the industry.

References

[1] G. Giustini, S. P. Walker, Y. Sato, and B. Niceno, "Computational fluid dynamics analysis of the transient cooling of the boiling surface at bubble departure," *Journal of Heat Transfer*, vol. 139, no. 9, Sep. 1, 2017, ISSN: 0022-1481. DOI: 10.1115/1.4036572 (cited on pp. 12, 17).

[2] G. Bartolomej and V. Chanturiya, "Experimental study of true void fraction when boiling subcooled water in vertical tubes," *Thermal Engineering*, vol. 14, no. 2, pp. 123–128, 1967. [Online]. Available: https://www.scopus.com/inward/record.uri?eid=2-s2.0-0001389457&partnerID=40&md5=cc7886a5df7b4b6a03d1e91ce0818b42 (cited on pp. 12, 33).

[3] J. Feng, Z. Skirpan, and E. Baglietto, "Toward industrial applicability of DNB predictions in CFD with improved wall boiling models," in *Volume 1: Beyond Design Basis; Codes and Standards; Computational Fluid Dynamics (CFD); Decontamination and Decommissioning; Nuclear Fuel and Engineering; Nuclear Plant Engineering*, American Society of Mechanical Engineers, Aug. 4, 2020, ISBN: 978-0-7918-8376-1. DOI: 10.1115/ICONE2020-16080 (cited on p. 12).

[4] T.-W. Ha, J. J. Jeong, and B.-J. Yun, "Improvement of the MARS subcooled boiling model for a vertical upward flow," *Nuclear Engineering and Technology*, vol. 51, no. 4, pp. 977–986, Jul. 1, 2019, ISSN: 1738-5733. DOI: 10.1016/j.net.2019.01.001. [Online]. Available: https://www.sciencedirect.com/science/article/pii/S1738573318308489 (cited on p. 12).

[5] G. Giustini, "Modelling of boiling flows for nuclear thermal hydraulics applications—a brief review," 2020 (cited on pp. 12, 18).

[6] G. Yadigaroglu, "CMFD and the critical-heat-flux grand challenge in nuclear thermal–hydraulics – a letter to the editor of this special issue," *International Journal of Multiphase Flow*, vol. 67, pp. 3–12, Dec. 2014, ISSN: 03019322. DOI: 10.1016/j.ijmultiphaseflow.2014.07.011 (cited on p. 13).

[7] H. Glaeser, "GRS method for uncertainty and sensitivity evaluation of code results and applications," *Science and Technology of Nuclear Installations*, vol. 2008, pp. 1–7, 2008, ISSN: 1687-6075. DOI: 10.1155/2008/798901 (cited on pp. 13, 23–27, 48, 51, 60).

[8] D. Bestion, D. Bestion, A. d. Crecy, *et al.*, "Review of uncertainty methods for CFD application to nuclear reactor thermalhydraulics," *null*, 2016. DOI: null (cited on pp. 14, 23).

[9] B. Koncar, E. Krepper, and Y. Egorov, "CFD modelling of subcooled flow boiling for nuclear engineering applications," presented at the Proceedings of the International Conference Nuclear Energy for New Europe 2005, Slovenia: Nuclear Society of Slovenia, 2005, 114Megabytes, ISBN: 961-6207-25-3. [Online]. Available: http://inis.iaea.org/search/search.aspx?orig_q=RN:37104707 (cited on p. 14).

[10] R. Zhang, T. Cong, W. Tian, S. Qiu, and G. Su, "Cfd analysis on subcooled boiling phenomena in pwr coolant channel," *Progress in Nuclear Energy*, vol. 81, pp. 254–263, 2015, ISSN: 0149-1970. DOI: https://doi.org/10.1016/j.pnucene.2015.02.005. [Online]. Available: https://www.sciencedirect.com/science/article/pii/S0149197015000396 (cited on p. 14).

[11] S. Rezaeiravesh, R. Vinuesa, and P. Schlatter, "An uncertainty-quantification framework for assessing accuracy, sensitivity, and robustness in computational fluid dynamics," *Journal of Computational Science*, vol. 62, p. 101 688, 2022, ISSN: 1877-7503. DOI: https://doi.org/10.1016/j.jocs.2022.101688. [Online]. Available: https://www.sciencedirect.com/science/article/pii/S1877750322000941 (cited on p. 14).

[12] M. Colombo and M. Fairweather, "Accuracy of eulerian–eulerian, two-fluid CFD boiling models of subcooled boiling flows," *International Journal of Heat and Mass Transfer*, vol. 103, pp. 28–44, Dec. 2016, ISSN: 00179310. DOI: 10.1016/j.ijheatmasstransfer.2016.06.098 (cited on p. 18).

[13] Z. Hózer, "Simulation of leaking fuel rods in a vver reactor," *Annals of Nuclear Energy*, vol. 70, pp. 122–129, 2014 (cited on p. 19).

[14] B. Han, X. Zhu, B.-W. Yang, S. Liu, and A. Liu, "Verification and validation of cfd and its application in pwr fuel assembly," *Progress in Nuclear Energy*, vol. 154, p. 104 485, 2022 (cited on p. 19).

[15] Q. Su, X. Du, G. Zhang, *et al.*, "Investigation on the dnb-type critical heat flux in a fuel assembly with 5 by 5 rods," *Applied Thermal Engineering*, p. 120 894, 2023 (cited on p. 19).

[16] G. Yadigaroglu, "Computational fluid dynamics for nuclear applications: From CFD to multi-scale CMFD," *Nuclear Engineering and Design*, vol. 235, no. 2, pp. 153–164, Feb. 2005, ISSN: 00295493. DOI: 10.1016/j.nucengdes.2004.08.044 (cited on p. 19).

[17] C. Boyd, "Perspectives on cfd analysis in nuclear reactor regulation," *Nuclear Engineering and Design*, vol. 299, pp. 12–17, 2016 (cited on p. 20).

[18] N. Kurul and M. Z. Podowski, "MULTIDIMENSIONAL EFFECTS IN FORCED CONVECTION SUBCOOLED BOILING," 1990 (cited on pp. 20, 26, 33, 48, 86).

[19] *An Evaluation of the RPI Model for the Prediction of the Wall Heat Flux Partitioning in Subcooled Boiling Flows*, vol. Volume 5: Innovative Nuclear Power Plant Design and New Technology Application; Student Paper Competition, International Conference on Nuclear Engineering, Jul. 2014, V005T17A014. DOI: 10.1115/ICONE22-30125. eprint: https://asmedigitalcollection.asme.org/ICONE/proceedings-pdf/ICONE22/45950/

V005T17A014/4249598/v005t17a014-icone22-30125.pdf. [Online]. Available: https://doi.org/10.1115/ICONE22-30125 (cited on p. 20).

[20] "Scala graduum caloris. calorum descriptiones i& signa," *Philosophical Transactions (1683-1775)*, vol. 22, pp. 824–829, 1700, ISSN: 02607085. [Online]. Available: http://www.jstor.org/stable/102813 (visited on 09/02/2023) (cited on p. 21).

[21] R. W. Bowring, "Physical model, based on bubble detachment, and calculation of steam voidage in he sub-cooled region of a heated channel," Dec. 1962. [Online]. Available: https://www.osti.gov/biblio/4759604 (cited on p. 21).

[22] B. B. Mikić and W. M. Rohsenow, "A new correlation of pool-boiling data including the effect of heating surface characteristics," *Journal of Heat Transfer-transactions of The Asme*, vol. 91, pp. 245–250, 1969. [Online]. Available: https://api.semanticscholar.org/CorpusID:119412060 (cited on p. 22).

[23] V. H. Del Valle and D. Kenning, "Subcooled flow boiling at high heat flux," *International Journal of Heat and Mass Transfer*, vol. 28, no. 10, pp. 1907–1920, 1985, ISSN: 0017-9310. DOI: https://doi.org/10.1016/0017-9310(85)90213-3. [Online]. Available: https://www.sciencedirect.com/science/article/pii/0017931085902133 (cited on p. 22).

[24] J. S. Murallidharan, B. Prasad, B. Patnaik, G. Hewitt, and V. Badalassi, "Cfd investigation and assessment of wall heat flux partitioning model for the prediction of high pressure subcooled flow boiling," *International Journal of Heat and Mass Transfer*, vol. 103, pp. 211–230, 2016 (cited on p. 22).

[25] A. de Crécy, P. Bazin, H. Glaeser, *et al.*, "Uncertainty and sensitivity analysis of the LOFT l2-5 test: Results of the BEMUSE programme," *Nuclear Engineering and Design*, vol. 238, no. 12, pp. 3561–3578, Dec. 1, 2008, ISSN: 0029-5493. DOI: 10.1016/j.nucengdes.2008.06.

004. [Online]. Available: https://www.sciencedirect.com/science/article/pii/S0029549308002793 (cited on p. 24).

[26] H. Glaeser, E. Hofer, M. Kloos, and T. Skorek, "Uncertainty and sensitivity analysis of a post-experiment calculation in thermal hydraulics," *Reliability Engineering I& System Safety*, vol. 45, no. 1, pp. 19–33, 1994, ISSN: 0951-8320. DOI: https://doi.org/10.1016/0951-8320(94)90073-6. [Online]. Available: https://www.sciencedirect.com/science/article/pii/0951832094900736 (cited on p. 24).

[27] D. Bestion, D. Bestion, A. d. Crecy, *et al.*, "Review of uncertainty methods for CFD application to nuclear reactor thermalhydraulics," *null*, 2016. DOI: null (cited on p. 24).

[28] S. S. Wilks, "Statistical prediction with special reference to the problem of tolerance limits," *The Annals of Mathematical Statistics*, vol. 13, no. 4, pp. 400–409, Dec. 1, 1942. DOI: 10.1214/aoms/1177731537. [Online]. Available: https://doi.org/10.1214/aoms/1177731537 (cited on pp. 24, 48).

[29] ——, "Determination of sample sizes for setting tolerance limits," *The Annals of Mathematical Statistics*, vol. 12, no. 1, pp. 91–96, Mar. 1, 1941. DOI: 10.1214/aoms/1177731788. [Online]. Available: https://doi.org/10.1214/aoms/1177731788 (cited on p. 24).

[30] M. A. Rahman, "Computational fluid dynamics of a nuclear reactor fuel channel," Master of Science thesis, Imperial College London, London, Sep. 2021, 95 pp. (cited on pp. 26, 52, 55, 63, 65).

[31] D. o. S. United States, *Annex i – nuclear-related measures*, 2017. [Online]. Available: United%20States,%20D.%20of%20S.%20(2017)%20Annex%20I%20%E2%80%93%20nuclear-related%20measures.%20Available%20at:%20https://2009-2017.state.gov/documents/organization/245318.pdf%20(Accessed:%2027%20June%202023). (cited on pp. 26, 36, 56, 81).

[32] MATLAB. "One-sample kolmogorov-smirnov test," kstest. (), [Online]. Available: https://uk.mathworks.com/help/stats/kstest.html#btnf4dh-ksstat (cited on pp. 27, 28, 51).

[33] K. Pearson, "Note on Regression and Inheritance in the Case of Two Parents," *Proceedings of the Royal Society of London Series I*, vol. 58, pp. 240–242, Jan. 1895 (cited on p. 28).

[34] C. Spearman, "The proof and measurement of association between two things," *The American Journal of Psychology*, vol. 15, no. 1, pp. 72–101, 1904, ISSN: 00029556. [Online]. Available: http://www.jstor.org/stable/1412159 (visited on 09/04/2023) (cited on p. 28).

[35] O. Marfaing, M. Guingo, J. Laviéville, *et al.*, "Comparison and uncertainty quantification of two-fluid models for bubbly flows with neptune_cfd and star-ccm+," *Nuclear Engineering and Design*, vol. 337, pp. 1–16, 2018 (cited on p. 29).

[36] "Pressure dependence of bubble departure diameter for water," *International Communications in Heat and Mass Transfer*, vol. 10, no. 6, pp. 501–509, 1983, ISSN: 0735-1933. DOI: https://doi.org/10.1016/0735-1933(83)90057-X. [Online]. Available: https://www.sciencedirect.com/science/article/pii/073519338390057X (cited on pp. 29, 48, 84).

[37] M. Colombo, R. Thakrar, M. Fairweather, and S. P. Walker, "Assessment of semi-mechanistic bubble departure diameter modelling for the cfd simulation of boiling flows," *Nuclear Engineering and Design*, vol. 344, pp. 15–27, 2019, ISSN: 0029-5493. DOI: https://doi.org/10.1016/j.nucengdes.2019.01.014. [Online]. Available: https://www.sciencedirect.com/science/article/pii/S0029549318308215 (cited on p. 30).

[38] M. Colombo and M. Fairweather, "Prediction of bubble departure in forced convection boiling: A mechanistic model," *International Journal of Heat and Mass Transfer*, vol. 85, pp. 135–146, 2015, ISSN: 0017-9310. DOI: https://doi.org/10.1016/j.ijheatmasstransfer.

2015.01.103. [Online]. Available: https://www.sciencedirect.com/science/article/pii/S0017931015001118 (cited on p. 30).

[39] K. Ardron, G. Giustini, and S. Walker, "Prediction of dynamic contact angles and bubble departure diameters in pool boiling using equilibrium thermodynamics," *International Journal of Heat and Mass Transfer*, vol. 114, pp. 1274–1294, 2017, ISSN: 0017-9310. DOI: https://doi.org/10.1016/j.ijheatmasstransfer.2017.07.013. [Online]. Available: https://www.sciencedirect.com/science/article/pii/S0017931016343216 (cited on p. 30).

[40] R. Cole, "A photographic study of pool boiling in the region of the critical heat flux," *AIChE Journal*, vol. 6, no. 4, pp. 533–538, 1960. DOI: https://doi.org/10.1002/aic.690060405. eprint: https://aiche.onlinelibrary.wiley.com/doi/pdf/10.1002/aic.690060405. [Online]. Available: https://aiche.onlinelibrary.wiley.com/doi/abs/10.1002/aic.690060405 (cited on pp. 30, 48, 85).

[41] R. Situ, J. Tu, G. Yeoh, T. Hibiki, and G.-C. Park, "Assessment of effect of bubble departure frequency in forced convective subcooled boiling," in *Proceedings of the 16th Australasian Fluid Mechanics Conference*, D. Mee, P. Jacobs, M. Cleary, *et al.*, Eds., Australia: School of Engineering, The University of Queensland, 2007, pp. 848–855. [Online]. Available: https://eprints.qut.edu.au/11204/ (cited on p. 31).

[42] T. Hibiki and M. Ishii, "Active nucleation site density in boiling systems," *International Journal of Heat and Mass Transfer*, vol. 46, no. 14, pp. 2587–2601, 2003, ISSN: 0017-9310. DOI: https://doi.org/10.1016/S0017-9310(03)00031-0. [Online]. Available: https://www.sciencedirect.com/science/article/pii/S0017931003000310 (cited on pp. 31, 84).

[43] S. StarCCM+, *Eulerian: Wall boiling*, 2020. [Online]. Available: https://docs.sw.siemens.com/documentation/external/PL20200805113346338/en-US/userManual/userguide/

html/index.html?param=WXD84&authLoc=https://thesteveportal.plm.automation.siemens.com/AuthoriseRedirect#page/STARCCMP%2FGUID-B62D9930-4DDF-40F3-93C8-1FF0BA7CE047.html%23 (cited on pp. 32, 33, 44, 47, 55, 65, 84).

[44] D. G. IAEA, *Verification and monitoring in the islamic republic of iran in light of united nations security council resolution 2231 (2015)*, 2015. [Online]. Available: https://www.iaea.org/sites/default/files/23/06/gov2023-24.pdf (cited on p. 36).

[45] N. R. C. United States. "Criticality," NRC Library. (Feb. 15, 2023), [Online]. Available: https://www.nrc.gov/reading-rm/basic-ref/glossary/criticality.html (cited on p. 39).

[46] W. E. Ranz, "Evaporation from drops-i and-ii," *Chem. Eng. Progr*, vol. 48, pp. 141–146, 1952 (cited on p. 44).

[47] D. Hill, D. Wang, A. Gosman, and R. Issa, "Numerical prediction of bubble dispersion in shear layers," in *Third International Symposium on Multiphase Flow and Heat Transfer, Xian, China*, 1994, pp. 110–117 (cited on p. 45).

[48] A. Behzadi, R. Issa, and H. Rusche, "Modelling of dispersed bubble and droplet flow at high phase fractions," *Chemical Engineering Science*, vol. 59, no. 4, pp. 759–770, 2004. DOI: 10.1016/j.ces.2003.11.018 (cited on pp. 45, 48).

[49] A. Tomiyama, I. Kataoka, I. Zun, and T. Sakaguchi, "Drag coefficients of single bubbles under normal and micro gravity conditions," *JSME International Journal Series B Fluids and Thermal Engineering*, vol. 41, no. 2, pp. 472–479, 1998 (cited on p. 46).

[50] A. Tomiyama, H. Tamai, I. Zun, and S. Hosokawa, "Transverse migration of single bubbles in simple shear flows," *Chemical Engineering Science*, vol. 57, no. 11, pp. 1849–1858, 2002 (cited on p. 46).

[51] S. Lo and D. Zhang, "Modelling of break-up and coalescence in bubbly two-phase flows," *The Journal of Computational Multiphase Flows*, vol. 1, no. 1, pp. 23–38, 2009. DOI: 10.

1260/175748209787387106. eprint: https://doi.org/10.1260/175748209787387106. [Online]. Available: https://doi.org/10.1260/175748209787387106 (cited on pp. 47, 83).

[52] S. Lo and P. K. M. Rao, "Modelling of droplet breakup and coalescence in an oil-water pipeline," 2007. [Online]. Available: https://api.semanticscholar.org/CorpusID:123887780 (cited on pp. 47, 83).

[53] H. Alimoradi and M. Shams, "Optimization of subcooled flow boiling in a vertical pipe by using artificial neural network and multi objective genetic algorithm," *Applied Thermal Engineering*, vol. 111, pp. 1039–1051, Jan. 25, 2017, ISSN: 1359-4311. DOI: 10.1016/j.applthermaleng.2016.09.114. [Online]. Available: https://www.sciencedirect.com/science/article/pii/S1359431116317987 (cited on p. 69).

Appendices

A Preprocessing

This appendix includes all the equations, contours and data sets relevant to inputs that directly influence the CFD simulations, but are not part of the UQ procedure. Hence this data is common to all simulations.

A.1 Material Properties

All these equations are at a system pressure of 42000 pascals or 0.42MPa and a temperature of 45 degrees celsius.

Thermal Conductivity

$$\begin{gathered} 557.9175240461 + 1.954089(T) - 2.48382645E-2(T^2) + \\ 2.928157E-4(T^3) + 2.2635E-6(T^4) + 6.5E-9(T^5) = 0.632718 \end{gathered} \tag{24}$$

Viscosity

$$\begin{gathered} 1999.399999991 - 49.31233333T + 6.1178E-1(T^2) - \\ 3.7370667E-3(T^3) + 8.8E-6(T^4) = 0.000714745 \end{gathered} \tag{25}$$

Specific Heat Capacity

$$4243.6743029 - 1.5251505T + 0.0100079(T^2) - 5.12E-5(T^3) + 3.0E-7(T^4) = 4191.87 \tag{26}$$

Saturation Temperature

$$72.71999 + 3.48432E2(P) + 6.616187E2(P^2) + 7.23963E2(P^3) - 3.1237E2(P^4) = 379.68 \quad (27)$$

A.2 Heat Flux Inputs at Critical and ARO conditions

Height(cm)	Power (kW)	Linear power, W/cm	Heat Flux W/m2□
105	2.259	225.9	898827.6366
95	2.405	240.51	956958.9857
85	2.572	257.22	1023445.97
75	2.592	259.2	1031324.141
65	2.379	237.95	946773.0683
55	2.335	233.47	928947.7128
45	2.344	234.36	932488.9106
35	2.507	250.66	997344.5568
25	2.564	256.43	1020302.66
15	2.426	242.58	965195.2549
5	2.259	225.91	898867.4253

Table 6. Heat flux at Critical condition in the reactor at wall cladding

Height (cm)	Power (kW)	Linear power, W/cm	Heat Flux W/m2□
105	2.259	225.9	898827.6366
95	2.405	240.51	956958.9857
85	2.572	257.22	1023445.97
75	2.592	259.2	1031324.141
65	2.379	237.95	946773.0683
55	2.335	233.47	928947.7128
45	2.344	234.36	932488.9106
35	2.507	250.66	997344.5568
25	2.564	256.43	1020302.66
15	2.426	242.58	965195.2549

Table 7. Heat flux at ARO condition in the reactor at wall cladding

Core Elements	Cold	HZP	HFP (BOC)
Fuel average Temperature, 0 K	293.6	318.15	809.15
Clad average Temperature, 0 K	293.6	318.15	384.15
Core average Coolant/Moderator Temp., 0 K	293.6	318.15	324.85
Structural Materials Temperature, 0 K	293.6	318.15	324.85
Coolant inlet Temperature, 0 K	293.6	318.15	318.15
Coolant outlet Temperature, 0 K	293.6	318.15	331.55
Core average Coolant/Moderator press., bara	1	4.2	4.2

Table 8. KHRR material properties experimental data [31]

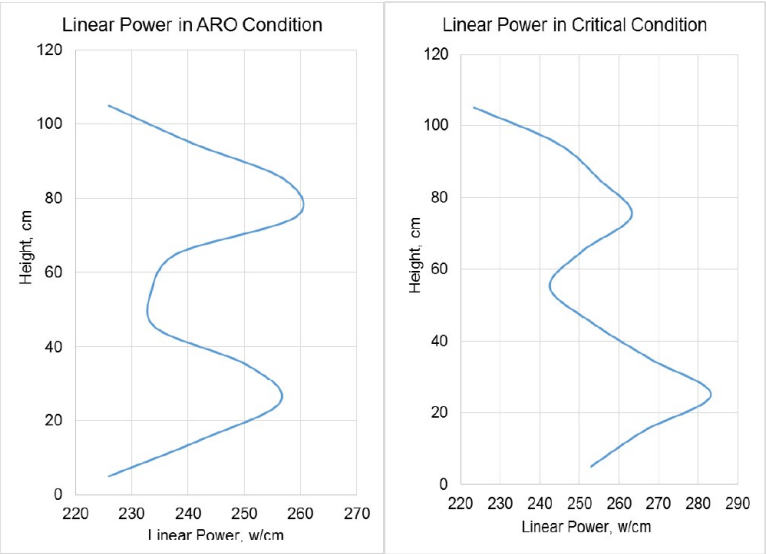

Fig. 32. Linear power from fuel cladding at ARO and critical conditions

B CFD Modelling

Turbulent Kinetic Energy (k)

$$\frac{\partial}{\partial t}(\rho k) + \frac{\partial}{\partial x_j}(\rho u_j k) = P_k - \rho\varepsilon + \frac{\partial}{\partial x_j}\left[(\mu + \frac{\mu_t}{\sigma_k})\frac{\partial k}{\partial x_j}\right] \tag{28}$$

Where:

- k is the turbulent kinetic energy
- ε is the turbulent dissipation rate
- u_j represents velocity in the j direction

- ρ is the density of the fluid
- P_k denotes turbulent production of kinetic energy
- μ is dynamic viscosity of the fluid
- μ_t is the turbulent viscosity
- σ_k and σ_ε are model constants

Turbulent Dissipation Rate (ε)

$$\frac{\partial}{\partial t}(\rho\varepsilon) + \frac{\partial}{\partial x_j}(\rho u_j \varepsilon) = C_{\varepsilon 1}\frac{\varepsilon}{k}P_k - C_{\varepsilon 2}\rho\frac{\varepsilon^2}{k} + \frac{\partial}{\partial x_j}\left[(\mu + \frac{\mu_t}{\sigma_\varepsilon})\frac{\partial \varepsilon}{\partial x_j}\right] \tag{29}$$

Where:

- k is the turbulent kinetic energy
- ε is the turbulent dissipation rate
- u_j represents velocity in the j direction
- ρ is the density of the fluid
- P_k denotes turbulent production of kinetic energy
- $C_{\varepsilon 1}$ and $C_{\varepsilon 2}$ are constants
- μ is dynamic viscosity of the fluid
- μ_t is the turbulent viscosity
- σ_ε is a model constant

S-Gamma model

$$S_\gamma = nM_\gamma = n\int_0^\infty d_p^\gamma P(d_p)d(d_p) \tag{30}$$

where:

- where:
- gamma is the order of the moment
- n is the number of particles per unit volume.
- d_p is the particle diameter
- $P(d_p)$ is the probability density function of particle diameter
- $d(d_p)$ is infinitesimal change in d_p[52][51]

C UQ sampling distribution

In this section values for calculation and sampling is given for each of the uncertainty quantification parameters.

C.1 Nucleation Site Density

Experimental Correlation given as:

$$n" = n''_{\text{avg}}(1 - e^{-\frac{\theta^2}{8\mu^2}})(e^{f(\rho^+)\lambda'/R_c} - 1) \tag{31}$$

This correlation gives the cavity density at different locations on the geometry. However we will be changing only the average cavity density which is given for reference as a value of 472000 /m^2 [42][43]. In table 9 the sampling dataset is given.

Case_x	NSD	Case_x	NSD	Case_x	NSD	Case_x	NSD
1	437955.2167	16	568008.6362	31	427837.1865	46	343852.9005
2	346096.8925	17	393741.4471	32	348223.3783	47	290980.1045
3	544118.0168	18	456003.6884	33	474802.9718	48	510917.5753
4	512650.0538	19	360187.2357	34	550919.3128	49	509072.3925
5	463708.9971	20	444512.7106	35	509397.6094	50	480801.6296
6	566469.6791	21	173003.2137	36	407185.4138	51	517948.4221
7	391147.8974	22	371445.0755	37	321157.9877	52	572118.4023
8	510364.0485	23	340039.9629	38	607066.2579	53	561776.4161
9	504234.4	24	378152.8551	39	661650.0684	54	419401.4584
10	504309.6309	25	452270.5884	40	483147.5466	55	546930.7596
11	404537.1164	26	441901.9792	41	380423.9056	56	488027.1664
12	502236.0895	27	651876.8232	42	582806.1985	57	425232.1053
13	424368.1456	28	419105.088	43	417173.1954	58	361606.9232
14	389069.4976	29	448869.4389	44	428537.7948	59	531851.4757
15	360685.299	30	326822.1549	45	553999.0371		

Table 9. Sample data set for nucleation site density

C.2 Bubble Departure Diameter

Experimental Correlation given as:

$$d_w = d_1 \cdot \theta \cdot \left(\frac{\sigma}{g \cdot \Delta p}\right)^{0.5} \cdot \left(\frac{\Delta p}{\rho_g}\right)^{0.9} \tag{32}$$

where,

$$d_1 = 0.002, \theta = 0.722, \sigma = 0.071, g = 9.81, \Delta p = 1070, \rho_g = 24.33$$

This correlation [36] gives the bubble departure diameter and gives the calculated experimental mean of value 0.000113133 m. In table 10 the sampling dataset is given.

Case_x	BDD	Case_x	BDD	Case_x	BDD	Case_x	BDD
1	0.000132734	16	0.000136063	31	0.0001039	46	0.0000912
2	0.00011713	17	0.000119598	32	0.000140289	47	0.0000871
3	0.000125347	18	0.0000959	33	0.000112167	48	0.0000749
4	0.000128277	19	0.000125699	34	0.000126047	49	0.000119524
5	0.00013909	20	0.0000825	35	0.0000908	50	0.0000778
6	0.000123685	21	0.000118554	36	0.000114564	51	0.000115577
7	0.000144447	22	0.000131059	37	0.000126444	52	0.000130585
8	0.000113634	23	0.000117857	38	0.0000829	53	0.000113084
9	0.000112072	24	0.000132639	39	0.00012084	54	0.000115198
10	0.000150858	25	0.000158342	40	0.000109101	55	0.000104748
11	0.000101831	26	0.00013362	41	0.0000923	56	0.0000803
12	0.00011307	27	0.000119052	42	0.000112301	57	0.000112161
13	0.00013353	28	0.000127361	43	0.0000711	58	0.000134438
14	0.000116455	29	0.000122568	44	0.0000659	59	0.000151676
15	0.000144286	30	0.000084	45	0.000087		

Table 10. Sample data set for bubble departure diameter

C.3 Bubble Departure Frequency

Experimental Correlation given as:

$$f = \left(\frac{4g(\rho_{\mathrm{L}} - \rho_{\mathrm{G}})}{3d_w \rho_{\mathrm{L}}} \right)^{0.5} \tag{33}$$

where,

$$g = 9.81, \rho_l = 1095, \rho_g = 24.33, d_w = 0.000113133$$

This correlation [40] gives the bubble departure diameter and gives the calculated experimental mean of value 338.497 /s. In table 11 the sampling dataset is given.

C.4 Bubble Influence Boiling Area Fraction

Experimental Correlation given as:

Case_x	BDF	Case_x	BDF	Case_x	BDF	Case_x	BDF
1	311.9173	16	280.390386	31	323.2279687	46	267.9704931
2	341.9872062	17	401.3817653	32	300.9175987	47	350.6257337
3	278.8958695	18	253.6871458	33	367.2866212	48	318.3392936
4	221.9540822	19	231.4280861	34	369.4672399	49	307.6893197
5	351.3941221	20	392.4228563	35	368.9754546	50	285.0311179
6	333.8263729	21	280.0264855	36	311.1537724	51	343.1154902
7	428.6207683	22	362.2477725	37	293.4532979	52	199.7344852
8	398.7563094	23	444.2178505	38	294.1811149	53	308.5566771
9	417.6676178	24	368.6471445	39	402.6525696	54	297.6417322
10	282.2084047	25	408.3740143	40	199.2174442	55	269.9550327
11	268.1189263	26	217.7984336	41	322.9152589	56	387.556457
12	243.1073227	27	388.2207306	42	358.8197156	57	283.3062125
13	375.9272309	28	499.2354493	43	289.4320995	58	379.1331622
14	548.1355798	29	379.1712195	44	374.3673264	59	411.8451343
15	393.184247	30	222.67846	45	333.1363276		

Table 11. Sample data set for bubble departure frequency

$$A_b = F_a \cdot \frac{\pi \cdot d_w^2}{4} \cdot n'' \tag{34}$$

where,

$$F_a = 0.9, \pi = 3.14, D_w = 0.000113133, n = 472000$$

This correlation [18] gives the bubble influence boiling area fraction and gives the calculated experimental mean value of 0.004270248. In table 12 the sampling dataset is given.

Once the data has been taken from the data sampling, a basic verification and validation process is executed with the actual confidence level being calculated from the data. The calculated confidence levels are shown in table 13. The equations used to calculate the actual confidence level achieved in the sampling, the following equation is used in MATLAB.

$$ActualConfidence = \frac{\sum(|(Sample - MeanValue)| < 1.96\sigma)}{59} \tag{35}$$

Case_x	BAF	Case_x	BAF	Case_x	BAF	Case_x	BAF
1	0.003923198	16	0.003402459	31	0.005775504	46	0.004449931
2	0.005870654	17	0.003552893	32	0.004172421	47	0.00595317
3	0.003943084	18	0.004128071	33	0.004002259	48	0.004291636
4	0.004612714	19	0.004109831	34	0.004954471	49	0.00452828
5	0.003314089	20	0.003545601	35	0.004680488	50	0.003484979
6	0.003747266	21	0.004421455	36	0.004910727	51	0.005671488
7	0.003292082	22	0.005330273	37	0.004921631	52	0.004374857
8	0.004598815	23	0.004060031	38	0.003031302	53	0.004713918
9	0.005359827	24	0.004099032	39	0.004722507	54	0.003473411
10	0.003773398	25	0.002427677	40	0.004193634	55	0.004985042
11	0.004635474	26	0.003622017	41	0.003633952	56	0.004595945
12	0.00384812	27	0.003104144	42	0.003689741	57	0.003302729
13	0.004355707	28	0.003946988	43	0.005342768	58	0.004303509
14	0.005271454	29	0.004710139	44	0.003592535	59	0.003893118
15	0.004370919	30	0.005545153	45	0.003235089		

Table 12. Sample data set for bubble influence boiling area fraction

Parameter	Actual Confidence Level
Nucleation Site Density	0.9661
Bubble Departure Diameter	0.9661
Bubble Departure Frequency	0.9661
Boiling Area Fraction	0.98305

Table 13. Calculated actual confidence level of input uncertainty parameters

The sampled data then is assorted into bins to compare against the actual gaussian distribution generated for the mean value and a standard deviation of 2.5 as shown in figure 33.

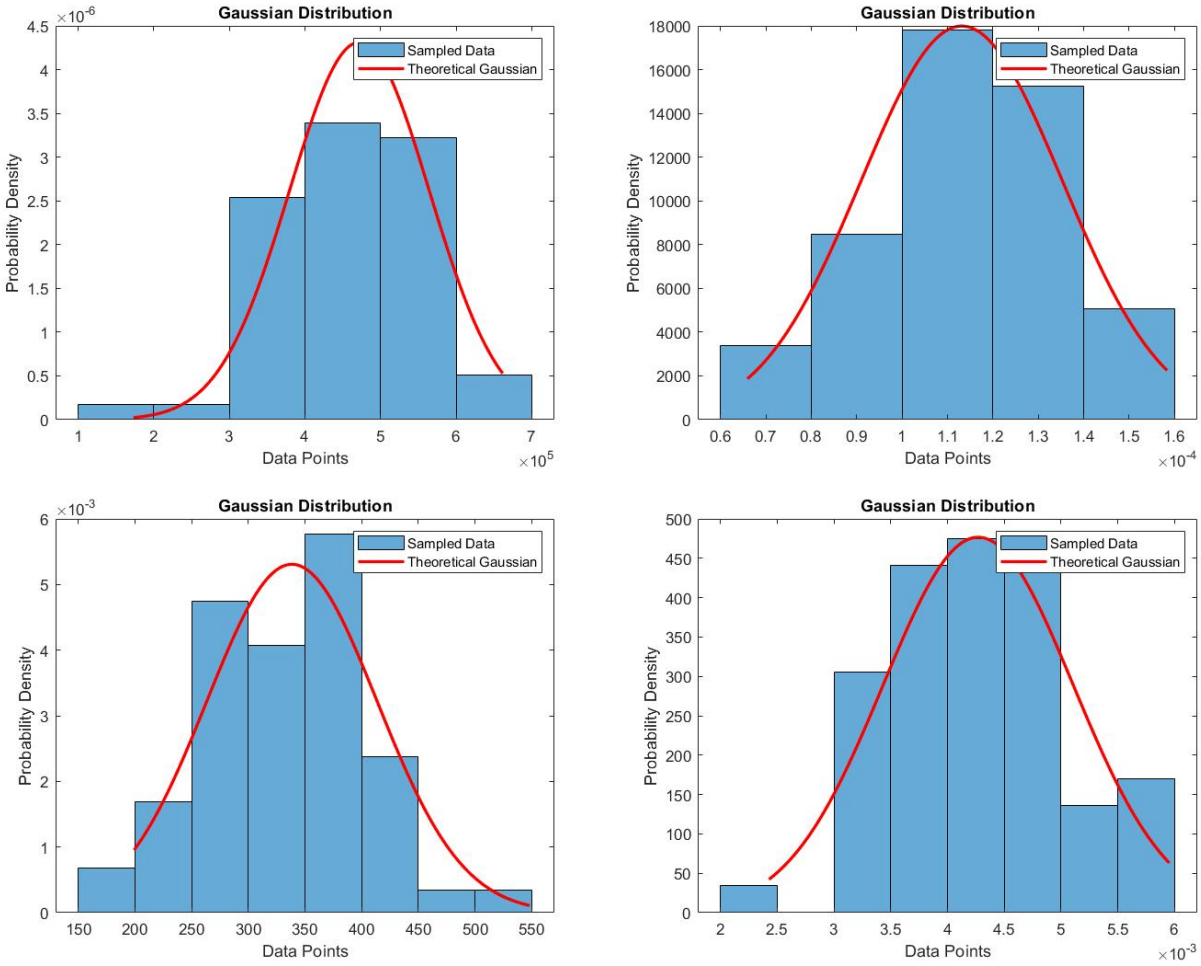

Fig. 33. UQ parameter sampling distribution for each of the 59 cases for UQ parameters, with the theoretical gaussian distribution (red) taken for reference

D UQ Results

UQ Parameter	Pearson	Spearman
Nucleation Site Density	-0.276	-0.2368
Bubble Departure Diameter	-0.7932	-0.8372
Bubble Departure Frequency	-0.3696	-0.5279
Boiling Area Fraction	0.24	0.1776

Table 14. Calculated correlation coefficients for pearson and spearman methods for sensitivity analysis for critical condition

UQ Parameter	Pearson	Spearman
Nucleation Site Density	-0.3012	-0.2354
Bubble Departure Diameter	-0.8674	-0.8382
Bubble Departure Frequency	-0.4364	-0.5255
Boiling Area Fraction	0.2494	0.1746

Table 15. Calculated correlation coefficients for pearson and spearman methods for sensitivity analysis for ARO condition

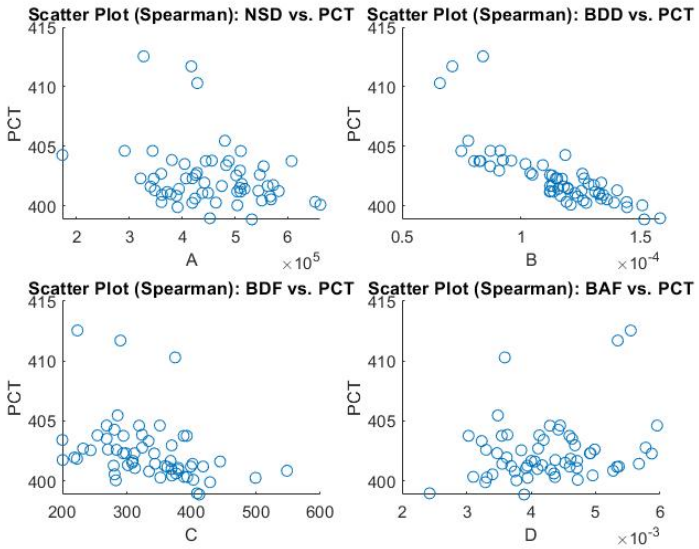

Fig. 34. Spearman Correlation plot between the UQ parameters and peak cladding temperatures for critical condition

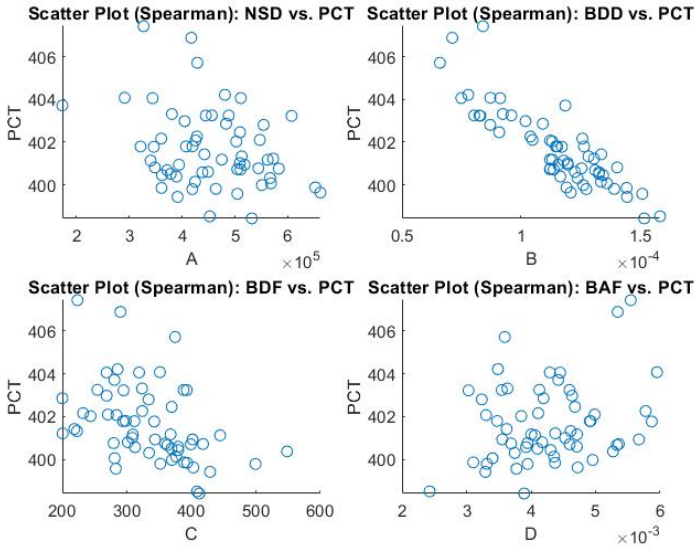

Fig. 35. Spearman Correlation plot between the UQ parameters and peak cladding temperatures for ARO condition